Chem Soc Rev

REVIEW ARTICLE

View Article Online
View Journal | View Issue

Cite this: *Chem. Soc. Rev.*, 2025, **54**, 4922

Chiral nanographenes exhibiting circularly polarized luminescence

Viksit Kumar, José L. Páez, Sandra Míguez-Lago, Juan M. Cuerva, Carlos M. Cruz * and Araceli G. Campaña *

Chiral nanographenes constitute an unconventional material class that deviates from planar graphene cutouts. They have gained considerable attention for their ability to exhibit circularly polarized luminescence (CPL), which offers new opportunities in chiral optoelectronics. Their unique π-conjugated architectures, coupled with the ability to introduce chirality at the molecular level, have made them powerful contenders in developing next-generation optoelectronic devices. This review thoroughly explores recent advances in the synthesis, structural design, and CPL performance of chiral nanographenes. We delve into diverse strategies for inducing chirality, including covalent functionalization, helically twisted frameworks, and heteroatom doping, each of which unlocks distinct CPL behaviors. In addition, we discuss the mechanistic principles governing CPL and future directions in chiral nanographenes to achieve high dissymmetry factors (g_{lum}) and tunable emission properties. We also discuss the key challenges in this evolving field, including designing robust chiral frameworks, optimizing CPL efficiency, and scaling up real-world applications. Through this review, we aim to shed light on recent developments in the bottom-up synthesis of structurally precise chiral nanographenes and evaluate their impact on the growing domain of circularly polarized luminescent materials.

Received 30th January 2025

DOI: 10.1039/d4cs00745j

rsc.li/chem-soc-rev

1. Introduction

Carbon-based materials are fundamental to modern science and technology due to their exceptional properties.[1] The carbon atom can form extended networks held together by covalent bonds in diverse orbital hybridizations, resulting in a wide range of materials with unique mechanical, electrical, and chemical characteristics. The versatility and abundance of carbon make it ideal for developing next-generation materials addressing key challenges in energy, sustainability, and high-performance electronics.[2–4] Two naturally occurring allotropes of carbon are diamond, solely containing sp^3-hybridized carbon atoms, and graphite, which is only formed by sp^2-hybridized carbon atoms, both in their pristine forms. Besides, other carbon allotropes such as fullerenes, carbon nanotubes, and graphene were all discovered in quick succession in the late 20th and early 21st centuries.[5] The story of graphene dates back to 1947 when Wallace began his theoretical investigation on single-layer graphene.[6] However, it was not until 2004 that Novoselov and Geim isolated and identified it for the first time, for which they got the 2010 Nobel Prize in Physics.[7] Each carbon atom in graphene is bonded to its three nearest neighbours by hybridization of the 2s, $2p_x$, and $2p_y$ atomic orbitals into sp^2 molecular orbitals, while the $2p_z$ orbitals create delocalized π and π* bands that are perpendicular to the graphene plane. This seemingly simple structure results in a unique combination of physical properties[8] and countless possible applications.[9] From its high conductivity and resistance to its flexibility and transparency, graphene brings together a whole range of uses in sensors, nano-electronic devices, spin devices, catalysis, and energy storage and it has thus been the subject of extensive experimental and theoretical research[10] over the last twenty years.[11]

Concerning its optical properties, graphene absorbs a considerable fraction of incident white light (2.3%) despite being only one-atom thick.[12] Photoluminescence in graphene, on the other hand, requires opening a bandgap in its electronic structure, which can be reached by the application of strain, an electric field or by reducing its size to the nanometric scale. In this sense, bottom-up synthesis comes into play, enabling the synthesis of small graphene cutouts with structural precision.[13,14] Nanographenes (NGs), a large category of polycyclic conjugated hydrocarbon (PCH) structures, are roughly described as finite graphenic units made of fused six-membered rings with sp^2 hybridized carbon atoms. NGs themselves have been the subject of substantial research, hand in hand with the goal of discovering bottom-up synthetic pathways to manufacture defect-free single-layered graphene sheets.

Department of Organic Chemistry, Unidad de Excelencia de Química (UEQ), Faculty of Sciences, University of Granada. Avda. Fuente Nueva s/n, 18071 Granada, Spain. E-mail: cmorenoc@ugr.es, araceligc@ugr.es

Following the classification made by Müllen and co-workers, NGs are considered graphene fragments between 1 and 100 nm (Fig. 1),[15,16] including graphene molecules (fragments between 1 and 5 nm in diameter), graphene nanoribbons (fragments between 5 and 10 nm in length), and graphene quantum dots for fragments below 100 nm. Since the seminal work in the late 1950s by Clar[17,18] and Halleux,[19] with the synthesis of the flagship NG, hexa-*peri*-hexabenzocoronene (HBC), much work has been done on the bottom-up synthesis of well-defined NGs, following in the footsteps of pioneers such as Müllen.[20,21]

More recently, designing non-planar, twisted, or contorted objects with inherent chirality has received major attention in the search of their intriguing properties. These chiral, non-planar NGs have been synthesized using a variety of methodologies like Scholl cyclodehydrogenation and alkyne-based approaches.[22–24] In the context of creating twisted structures, Miao and co-workers recent review of Scholl chemistry highlights its extensive use in producing chiral NGs.[25] Chirality can be introduced in NGs through various strategies,[26] being one of the most widely employed the inclusion of twisted or helical motifs in its structure.[27,28] Another approach involves the incorporation of chiral auxiliaries or substituents into NG frameworks, leading to asymmetry. In addition, axial or point chirality can be introduced by chemical modification of the edges or peripheries[28] of NGs with chiral groups or ligands.[29–32] In parallel, researchers have also explored the construction of twisted or saddle-shaped NGs containing non-benzenoid rings and heteroatoms, which exhibit intrinsic chirality due to the breaking of their symmetry.[20]

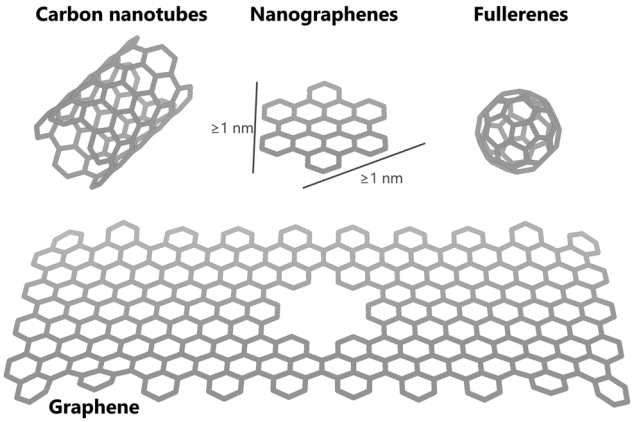

Fig. 1 Structures of carbon nanotubes, fullerenes, graphene and nanographenes.

Chiral NGs allow the differential interaction of each enantiomer with circularly polarized light, through which their

From left to right: Juan M. Cuerva, Carlos M. Cruz, Araceli G. Campaña, José L. Páez, Sandra Míguez-Lago and Viksit Kumar.

Viksit Kumar *obtained his MSc (Chemistry) from the Indian Institute of Technology (ISM), Dhanbad, India, in 2017. In 2018, he started his doctoral study under the supervision of Dr Santhosh Babu Sukumaran at the National Chemical Laboratory (CSIR-NCL) Pune, India. He joined the NanographOUT team at the University of Granada in 2024 as a Postdoctoral researcher.* ***José L. Páez*** *was born in Algeciras (Cádiz, Spain) in 1999. He obtained his BSc (2021) and his MSc (2023) in Chemistry at the University of Granada under the supervision of Prof. Juan M. Cuerva and Dr. Carlos M. Cruz. He joined the MOReFUN group in 2023 as PhD student under the supervision of Dr. Carlos M. Cruz and Prof. Araceli G. Campaña.* ***Sandra Míguez-Lago*** *completed her PhD studies in 2016 as a Xunta de Galicia Fellow at the University of Vigo (Spain), under the supervision of Profs. Magdalena Cid and José Lorenzo Alonso-Gómez. She moved to the University of Erlangen-Nürnberg (Germany), as a postdoctoral researcher where she worked with Prof. Milan Kivala, supported by the FFL and ETI funding programs. She joined the University of Granada as Junta de Andalucía Fellow. Since 2024, she holds an Assistant Professor position, working within the MOReFUN research group.* ***Juan M. Cuerva*** *graduated in Chemistry from the University of Granada (1992) in two specialties: Organic Chemistry and Technical Chemistry. He got his PhD from the University Autonomous of Madrid in 1997 under the supervision of Prof. A. M. Echavarren. In 1998, he joined the staff of the University of Granada, currently as full Professor in the MOReFUN research group. In 2015 he was awarded the ''Ignacio Ribas'' Medal, from the Specialized Group on Organic Chemistry of the Royal Spanish Chemistry Society.* ***Carlos M. Cruz*** *is Ramón y Cajal Researcher at the Department of Organic Chemistry of the University of Granada and leads the SPIRANT team within the MOReFUN Group. He received his PhD in 2020 under the supervision of Prof. Araceli G. Campaña and Prof. Juan M. Cuerva. He joined the group of Prof. Michal Juríček at the University of Zurich as a postdoctoral fellow before being appointed as Junta de Andalucía Postdoctoral Researcher in 2022 at the University of Granada.* ***Araceli G. Campaña*** *is an Associate Professor in the Department of Organic Chemistry at the University of Granada, where she leads the NanographOUT team within the MOReFUN Group. She earned her PhD in Chemistry from the UGR in 2008 under the supervision of Prof. Juan M. Cuerva and Prof. J. Enrique Oltra. Following postdoctoral research at the University Autonomous of Madrid (Prof. Diego J. Cárdenas group) and the University of Edinburgh (Prof. David A. Leigh group), she held the Ramón y Cajal research position at the UGR before taking her current academic appointment in 2020.*

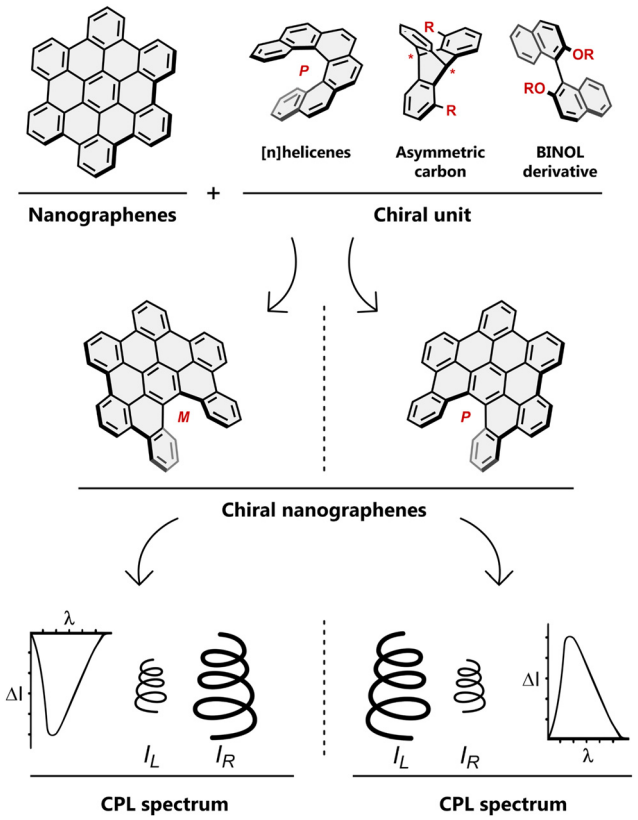

Fig. 2 Structural motifs that furnish chiral nanographenes, schematic representation of a pair of enantiomeric chiral nanographenes (seco-HBC) and their opposite CPL spectra.

chiroptical properties can be explored. Among them, circularly polarized luminescence (CPL) represents a promising property, with applications in sensing, organic electronics, bioimaging, encryption, *etc.*[33–37]

At the electronic level, the coupling between electronic transitions and chiral geometry can result in large chiroptical responses, enhancing the degree of circular polarization. This interplay between structure and CPL performance is a key area of investigation as researchers seek to design NGs that optimize luminescence efficiency and CPL intensity.

Picking up on the variety of chiroptical properties it is necessary to describe the light-matter interplay. At the very moment polarized light penetrates the sample and interacts with the chiral NGs, such light can be either right or left circularly polarized, depending on whether the accompanying electromagnetic vector is a clockwise or counterclockwise spiral. To this regard, the enantiopure NGs show differential absorption of left and right circularly polarized light, which can usually be used to gain information on the chirality of the ground state. In the same manner, this can be applied to the study of aggregates, supramolecular systems and intramolecular interactions.[38] Mathematically, CD can be defined by eqn (1.1), being A_L and A_R the absorption of left and right circularly polarized light, respectively. We refer to either electronic CD (ECD) when we measure it in the ultraviolet-visible region or to vibrational CD (VCD) when it appears in the infrared region.

$$\mathrm{CD} = A_L - A_R \tag{1.1}$$

Circular dichroism can turn into a value independent of the sample concentration, when expressed in extinction coefficient units (ε), analogously to the Lambert–Beer law, (eqn (1.2)) being c the concentration and b the optical pathlength.

$$\Delta\varepsilon = \varepsilon_L - \varepsilon_R = \frac{\mathrm{CD}}{c \cdot b} \tag{1.2}$$

Nevertheless, in order to be able to compare the CD response of compounds with different ε, a dimensionless magnitude, named the absorption dissymmetry factor g_{abs}, is employed (eqn (1.3)):

$$g_{abs} = \frac{\varepsilon_L - \varepsilon_R}{\frac{1}{2}(\varepsilon_L + \varepsilon_R)} = \frac{\Delta\varepsilon}{\varepsilon} \tag{1.3}$$

In chiral NGs, different enantiomers emit left-handed and right-handed circularly polarized light with varying intensities under incident light, which reflects the chirality of the NGs in the excited state (Fig. 2). Generally, chirality and fluorescence are two mandatory elements for achieving intrinsic CPL. Parallel to absorption, in emission, the first criterion for evaluating the quality of CPL is the luminescence dissymmetry factor (g_{lum}) (eqn (1.4)).

$$g_{lum} = \frac{I_L - I_R}{\frac{1}{2}(I_L + I_R)} \tag{1.4}$$

This factor depends on the molecular symmetry, the momenta components of the electronic transitions involved, and the strength of the coupling between them, being I_L and I_R the left and right circularly polarized fluorescence intensities, respectively. Both g_{abs} and g_{lum} values should fall between -2 and 2 by definition, while $g = 0$ indicates null discrimination in terms of circular polarization of the absorbed/emitted light. In addition, both g factors can also be predicted theoretically. Whilst for g_{abs}, it can be calculated for each $S_0 \rightarrow S_n$ transition, for g_{lum}, one should consider that in emission, usually solely the transition from the first excited state to the ground state of a molecule ($S_1 \rightarrow S_0$) is computed. Besides, both g factors can be calculated from the associated rotatory (R) and dipolar strengths (D) of a certain transition, or, in other words, from the dipole magnetic (m) and electric (μ) moments for a given transition, along with the angle between them (θ) (eqn (1.5)).

$$g = \frac{4R}{D+G} = \frac{4|m||\mu|\cos\theta}{\left(|\mu|^2+|m|^2\right)} \tag{1.5}$$

Thus, careful examination of eqn (1.5) hints at the enormous influence of the dipole moments on the chiroptical response. Specially for small organic molecules, μ is usually larger than m; therefore, increasing m directly impacts both CD and CPL responses. Dissymmetry factors are, besides, dependent on an appropriate alignment of the moments, which should orient with each other with an angle θ close to either 0° or 180°.

Nevertheless, large g_{lum} values are not always synonymous with straightforward applicability of the compound in case the emitter presents a small fluorescence quantum yield. An example of that are lanthanide and d-block metal complexes in which transitions are metal-centered and electric dipole forbidden.[39,40]

To understand overall CPL efficiency, extra parameters other than g_{lum} are explained in literature. Example of that is the report of Mori and co-workers in 2020 were circular polarization luminosity (Λ_{CPL}) per single chiral molecule (eqn (1.6)) was proposed to get an intrinsic index for CPL efficiency.[41]

$$\Lambda_{CPL} = f \cdot \Phi_{lum} \cdot \frac{|g_{lum}|}{2} \quad (1.6)$$

Where f and Φ_{lum} are accounting for the efficiencies of light absorption (oscillator strength) and emission intensity, respectively. By definition, values of Λ_{CPL} lie between 0 and 1. Recently, Zinna and co-workers have described the CPL brightness (B_{CPL}) as another parameter to understand CPL efficiency, including the extinction coefficient and the fluorescence quantum yield, which can better assess on the practical application of a CPL emitter.[42]

$$B_{CPL} = \varepsilon_{\lambda} \cdot \Phi_{F} \cdot \frac{|g_{lum}|}{2} \quad (1.7)$$

In here, ε_{λ} is the extinction coefficient at the excitation wavelength, and Φ_F the fluorescence quantum yield.

In chiral NGs, CPL efficiency can be modulated by several factors, including the extent of π-conjugation, the rigidity of the molecular framework, and the degree of electronic coupling between chromophores.[43] For example, helical NGs with extended conjugation tend to exhibit higher g_{lum} values in comparison with their non-extended helical counterparts (simple helicenes) due to the strong interaction between the delocalized π-electron system and the chiral environment. Additionally, introducing functional groups that enhance electronic asymmetry can further improve the CPL performance, though fostering luminescence (typically by μ enhancement). Thus, what sets chiral NGs apart is their ability to combine the intrinsic optoelectronic properties of NGs with the chiroptical activity of chiral molecules, by introducing chirality into the planar or quasi-planar NG structure. By virtue of OLED display technologies raising, among others, CPL materials have become a research hotspot in the field of chiral materials and luminescent materials. Thus, the non-compiled outstanding achievements concerning NG-based CPL materials in the past years, claim for a review article, which is expected to promote further progress in this unique research area. To the best of our knowledge, though some general reviews focusing on the synthesis and applications of CPL emitters have been reported in the literature,[28,44–46] there is no report that primarily focuses on the chiral NGs as CPL emitters. This review summarizes the recent advances in the synthesis of chiral NGs-based CPL emitters, prepared through bottom-up synthesis. Reviews focusing on graphene quantum dots mostly prepared by top-down methodologies lacking well defined structures will be deliberately set aside, given their deficiency in understanding the pursued structure–property relationships at molecular level.[47–49] As NGs, we have chosen the aforementioned 1 × 1 nm size criteria from among the vast array of chiral polycyclic conjugated hydrocarbons. Furthermore, only chiral NG examples that have been described and reported their CPL emission have been included in this review. More importantly, this review will provide a detailed analysis of the influence of structural design on chiroptical properties under each section.

To understand the structure–property relationship in NGs as chiral emitters, we have included a final summary table with the most relevant optical and chiroptical data. Furthermore, the opportunities and challenges for achieving high-performance CPL emitters are also presented and discussed. This review will contribute to guide researchers in the design of new chiral NG-based CPL emitters for functional applications.

2. NGs as CPL emitters

2.1. Design and synthetic strategies

The synthesis of chiral NGs requires precise control over their π-conjugated core and the introduction of chirality.[50] Several synthetic strategies have been developed to achieve this goal, including the bottom-up synthesis of NG cutouts. In order to achieve that, there are several well-established synthetic approaches to prepare chiral NGs, including cyclodehydrogenation (mostly under Scholl conditions) of polycyclic conjugated hydrocarbons into larger NG structures. This reaction can be adapted to form twisted or helically chiral NGs by carefully choosing sterically hindered precursors and reaction conditions.[51–54]

Cross-coupling reactions (*e.g.* Suzuki, Sonogashira, Stille, Kumada) are commonly used for the introduction of various functional groups at specific positions on the NG core, allowing to generate prochirality into the structure. Recent advances in synthetic chemistry have also enabled the introduction of heteroatoms (such as nitrogen, sulphur, or boron) into the NG framework, which can further modulate the chiral and photophysical properties.[55,56] Due to the altered electronic structure, these heteroatom-doped chiral NGs exhibit enhanced luminescence and unique CPL characteristics. Moreover, researchers have explored the blend of NGs with inherently chiral scaffolds, such as chiral polymers and other dopants, to further enhance their CPL activity. Here we classify all different non-planar NGs into benzenoid, non-benzenoid and heteroatom-containing families.

2.1.1. Introducing chirality in planar NGs. The formation of tightly twisted or helical structures encounters high steric hindrance due to spatial limitations and repulsions between adjacent atoms or molecular groups. Strategically placing bulky substituents at specific positions on the NG periphery forcing the molecule to twist out of planarity constitutes a major strategy to induce chirality. For example, substituents like *tert*-butyl, silyl, or large aromatic groups can introduce steric crowding, which causes the NG to adopt a helical twist to relieve strain. Precise formation of the helical unit can be

controlled by strategically placing bulky groups, which results into steric repulsive effects that prevent complete planarization during the cyclodehydrogenation reaction. In 2020 Jux *et al.* reported an HBC-based twisted NG with [5]helicene.[57] In here, the helicity was introduced with the help of strategically placing *tert*-butyl groups sterically demanding that prevent a complete closure to planar PAHs during the oxidative cyclodehydrogenation step. Fusing rings orthogonally by duplication extra aromatic rings can introduce steric repulsion to form a helical spiral is a well-known strategy to synthesize chiral NGs. So, placing substituents on opposite edges of the NG core, especially near the centre or along specific symmetry-breaking positions, to induce steric hindrance that promotes helicity. This approach can be tuned to achieve different twist angles depending on the size and position of the substituents.[44,58]

2.1.2. Introducing non-benzenoid rings in NG core. Introducing non-benzenoid rings within the benzenoid nanographene core induces curvature due to the natural bending in these structures. These rings disrupt the planarity, creating a twisted structure with high structural distortions, inducing chirality and significantly altering the material's properties. Typically, NGs are comprised of hexagonal benzene rings, forming flat, planar structures. However, incorporating single five or seven-membered rings introduces strain and deviation from planarity. This deviation results in twisted or helical structures, imparting chirality to the achiral graphene plane. The ring induces a high degree of structural distortion, deep saddle curvature, and substantial torsion angles, possibly resulting in a high isomerization barrier and intriguing chiroptical properties.[59,60]

2.1.3. Introducing heteroatoms in NG core. Introducing heteroatoms into NG core is another strategy to modulate their electronic properties, stability, and chiroptical activity, making them more versatile for applications in circularly polarized luminescence (CPL), optoelectronics, and catalysis.[55,56] Replacing specific carbons in the NG backbone with heteroatoms (such as nitrogen, sulphur, selenium, oxygen, boron, and phosphorus) their inherent properties can be tuned. Designing helically chiral NGs with both electron-donating (*e.g.* nitrogen, sulphur) and electron-withdrawing (*e.g.* boron) heteroatoms helps create a donor–acceptor system. This can enhance CPL properties by inducing asymmetry in electronic transitions.[61] Incorporating heavy heteroatoms (such as selenium or iodine) at specific positions in helically chiral NGs increases spin–orbit coupling due to heavy atom effect which can alter luminescence properties and CPL response.[62] Recently Babu and co-workers reported sulphur- and selenium-containing helical NGs and shown the importance of heteroatom doping for altering the optical, chiroptical, and redox properties of the NGs.[63]

To conclude, the design of chiral NGs as CPL emitters hinges on creating a balance between structural chirality and electronic properties. Strategies such as introducing helical or twisted geometries, covalently attaching chiral groups, or using self-assembly techniques can lead to efficient CPL emission. Fine control over molecular size, edge structure, heteroatom doping, and functionalization enables the tuning of CPL properties, making NGs promising candidates for applications in chiral optoelectronics and sensing.

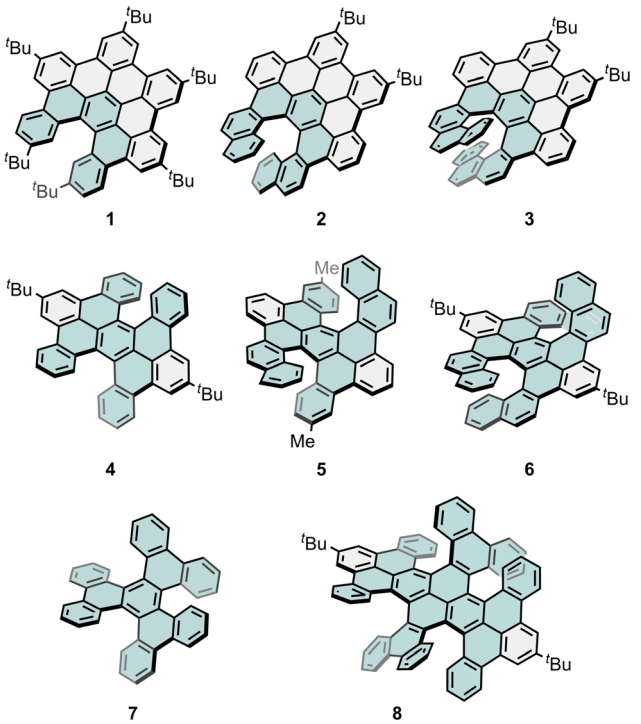

Fig. 3 Examples of embedded carbohelicenes into the HBC core (**1–3**), their double helicene analogues as extended peropyrenes (**4–6**), hexabenzotriphenylene as a triple helicene analogue of HBC (**7**), and chiral teropyrene-based nanographene (**8**).

2.2. NGs bearing benzenoid rings

This category of NGs comprises helically twisted π-extended NGs containing *ortho*-fused benzene ring systems, [*n*]helicenes, where *n* represents the number of the rings forming the helix. Chiral NGs bearing benzenoid rings represent a unique class of materials that combine the structural rigidity and extended π-conjugation of fused benzene rings with chirality. These NGs are not only defined by their polycyclic conjugated hydrocarbon frameworks but also by the introduction of chirality through helical structures and how all together assemble. According to our stablished criteria, *seco*-HBC, which is an HBC in which a benzenoid ring is cleaved to form a carbo[5]helicene, can be regarded as the simplest chiral NG (compound **1**, Fig. 3). Jux and co-workers reported its synthesis,[64] although an alternative synthesis and its chiroptical properties were recently investigated by Tanaka and co-workers.[65] Compound (*P*)-**1** was prepared *via* enantioselective synthesis using a combination of a $Ni(cod)_2$ catalysed [2+2+2] cycloaddition followed by a Scholl reaction. Compound (*P*)-**1** exhibits a Φ_F of 0.11 and a g_{lum} of 1×10^{-3} (B_{CPL} = 5 M^{-1} cm^{-1}). Structurally related with *seco*-HBC, there are examples of larger carbo[*n*]helicenes embedded into the structure of HBC with CPL responses. In this sense, Narita and co-workers reported the synthesis of compounds **2** and **3** (Fig. 3) by regioselective oxidative cyclodehydrogenation.[43] They represent chiral HBC analogues bearing a carbo[7] and

carbo[9]helicene, respectively. While **2** shows a $|g_{lum}|$ of 0.77×10^{-3} and a Φ_F of 0.25, **3** shows an improvement of one order of magnitude in the chiroptical response ($|g_{lum}| = 7.4 \times 10^{-3}$, $\Phi_F = 0.41$, and $B_{CPL} = 12.6\ M^{-1}\ cm^{-1}$) because of embedding a longer helicene in the structure which result in a larger internal area for the case of **3**. On the other hand, the higher Φ_F values of **2** and **3** compared with pristine [7]helicene and [9]helicene, whose Φ_F values account to 0.021 and 0.014, respectively,[66] clearly evidences the impact of the π-extension of the system in their emission performance.

Selected partially π-extended double helicenes **4** to **6** (Fig. 3) are included for comparison as they could be considered as double helical analogues of **1**. That is the case of tetrabenzoperopyrene (**4**, Fig. 3) as double carbo[5]helicene whose synthesis was reported by Clar and co-workers in 1959,[18] however, its CPL response was studied in 2024 by Hu and co-workers.[67] Compound **4** exhibits a high Φ_F of 0.81 (pristine peropyrene, $\Phi_F = 0.9$) and the measured $|g_{lum}|$ value of their isolated enantiomers reached a value of 0.53×10^{-3}. In 2018, Tanaka reported the synthesis of **5** (Fig. 3), as a partially π-extended double carbo[6]helicene.[68] It was synthesized by Rh(I)/binap-catalysed enantioselective intramolecular [2+2+2] cycloaddition of 2-phenylnaphthalene-linked triynes followed by posterior aromatization by Scholl oxidation. Compound **5** displayed a low $|g_{lum}|$ value of 0.75×10^{-3} and a remarkable $\Phi_F = 0.75$, which could be due to the location of the HOMO and LUMO orbitals in the central peropyrene core without the influence of the lateral helicenes. In fact, this *g* factor is very similar to the one previously reported for chiral peropyrenes with twisted backbones based on the steric congestion of bay regions and the inclusion of octagonal rings, synthetized by the groups of Chalifoux and Juríček ($|g_{lum}| = 0.7 \times 10^{-3}$ and 0.2×10^{-3}, respectively), respectively.[69,70] In 2017, Narita and co-workers reported the first X-shaped double carbo[7]helicene (compound **6**, Fig. 3) as a novel structural motif obtained by regioselective cyclodehydrogenation. The molecule showed promising $|g_{abs}|$ of 1.5×10^{-2} and high $\Phi_F = 0.8$, though its CPL property was not studied at that moment.[52] However, later on, in 2022 they reported a $|g_{lum}|$ of 0.07×10^{-3} and compared it with other N-doped X-shaped double [7]helicenes with different terminal heterocycles as compound **60** (Section 2.4.1, Fig. 15).[61,71] A comparison of the chiroptical responses of **1** *vs.* **4** or **2** *vs.* **6**, bearing one or two carbohelicenes of the same size, shows again how the inclusion of multiple helicene can result in a considerable decrease in the dissymmetry emission, in one order of magnitude ($|g_{lum}| = 1 \times 10^{-3}$ and 0.53×10^{-3} for **1** and **4**, respectively; $|g_{lum}| = 0.77 \times 10^{-3}$ and 0.07×10^{-3} for **2** and **6**, respectively). These examples reveal again that not always more helical moieties result in enhanced chiroptical responses and bring out attention to the fine design required for a better performance in well-defined NGs.

By combination of three pentahelicene units, Mori and co-workers synthesized hexabenzotriphenylene (compound **7**, Fig. 3). Compound **7** could resemble as a triple seco-HBC, where three benzenoid rings are cleaved.[72] The D_3-symmetry propeller-like structure was isolated, with the three carbo[5] helicenes in the same configuration. This compound was found stable towards undesirable racemization and degradation relative to pH change. Its Φ_F in CH_2Cl_2 is 0.018 and shows a g_{abs} ($S_0 \rightarrow S_1$ transition) and g_{lum} values of -1.8×10^{-3} and -1.3×10^{-3}, respectively, for (*P*,*P*,*P*)-**7**. It resulted that merging three pentahelicenes in a single structure gave significantly lower chiroptical response in comparison with pristine pentahelicene (-7.6×10^{-3} and -2.7×10^{-3}, for g_{abs} and g_{lum}, respectively) although with better photostability and lower excited-state relaxation.[72] This example reveals that special attention has to be paid to increase the chiroptical response by merging more than one helicene, required for a better performance.[73]

Moving from peropyrene to teropyrene-cored NGs, Chaolumen and co-workers described the preparation of compound **8** (Fig. 3).[74] The enantiopure samples of **8** were isolated, exhibiting the same configuration in all the [6]helicenes. Remarkably, the frontier molecular orbitals resemble those of pyrene, although with a lower HOMO–LUMO gap. Compound **8** exhibit a $\Phi_F = 0.58$ with an emission centred at 612 nm. The $|g_{lum}|$ value was evaluated as 0.78×10^{-3} with a $B_{CPL} = 6.8\ M^{-1}\ cm^{-1}$.

Using a perylene core, Wang and co-workers reported the synthesis of a chiral NG with luminescent properties by incorporating two lateral dibenzo[6]helicene fragments (compound **9**, Fig. 4).[75] In this case, a high Φ_F is expected due to the

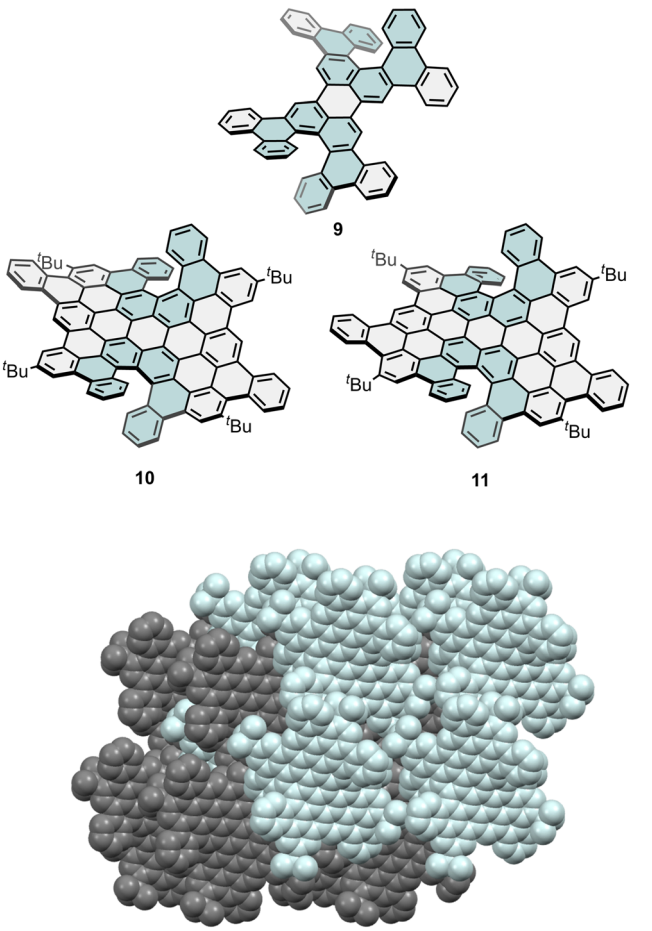

Fig. 4 Chiral perylene-cored nanographene **9** and its extended analogues **10** and **11**. Crystal packing of compound **10** (bottom).

distribution of the frontier molecular orbitals in the central part of the perylene core and together with a certain degree of orbital delocalization on the helicenes, which justifies the chiroptical activity. This compound exhibits a remarkably high Φ_F value of 0.93 among the previously reported chiral NGs and an excellent B_{CPL} of 32 M^{-1} cm^{-1}. In addition, the two enantiomers showed maximum $|g_{abs}|$ of 7.0 × 10^{-3} in the ECD spectrum and CPL with a $|g_{lum}|$ of 0.8 × 10^{-3}. As π-extended analogues of **9**, one can find other two examples bearing double carbo[6]helicenes as chiral NGs. Compounds **10** and **11** (Fig. 4), reported by Qiu and co-workers in 2022, reach a polyaromatic framework of 29 conjugated benzenoid rings.[76] In this case, an overcrowded perylene-cored oligophenylene is created by sequential regioselective Scholl reaction in the *peri*- and bay regions, forming the double carbo[6]helicene motif. The larger π-extension demonstrated a great effect in decreasing HOMO–LUMO gaps, and quasi-panchromatic absorption, along with intense, red-shifted emission was observed. Besides, CPL signal is centred at 625 nm with $|g_{lum}|$ values estimated to be 1.5 × 10^{-3}, and notably reaching 800 nm. Single crystals of **10** and **11** were grown in pentane/CS_2 mixtures, packing in the triclinic $P\bar{1}$ space group. Crystals of **10** consisted of intercalated layers of (*P*,*P*) and (*M*,*M*) enantiomers (Fig. 4). Compound **10** has a smaller helix pitch and interplanar angles (3.11–3.18 Å, 44.3–50.6°) compared to **11** (3.22–3.31 Å, 55.6–64.4°).

The perylene core has been also used as initial scaffold to construct perylene-HBC hybrids. Wu and co-workers reported the synthesis of a series of helical NGs (**12**, **13**, **14** and **15**, Fig. 5), where perylene is fused with one to four HBC subunits *via* Diels–Alder cycloaddition followed by Scholl reaction. X-Ray crystallographic analysis confirmed their structures, revealing helicene moieties integrated into a highly contorted framework and demonstrating respectable Φ_F values of 0.319, 0.150, 0.137, and 0.065, respectively, with emission maxima reaching 1010 nm. Besides, they evaluated the $|g_{abs}|_{max}$ at 292 nm (3.0 × 10^{-3}), 492 nm (8.5 × 10^{-3}), 454 nm (3.0 × 10^{-3}), and 604 nm (1.2 × 10^{-3}) for **12**, **13**, **14**, and **15**, respectively. Furthermore, the CPL spectra of enantiopure **12**, **13**, and **14** were also measured in toluene, displaying mirror images consistent with their emission profiles, and maximum $|g_{lum}|$ values of 4.5 × 10^{-3} for **12**, 1.3 × 10^{-3} for **13**, and 1.4 × 10^{-3} for **14**. However, they did not observe CPL signal in the NIR-II region for **15**.[77]

Belonging to this family of chiral NGs exhibiting multiple HBC units we can find the link of two (or more) HBCs by chiral moieties, leading to the family of bi or multilayer NGs (with simple carbohelicenes as hinge) or fully helical ribbon-shaped or propeller-shaped NGs (with π-extended helicenes as link) some of which bearing heteroatoms or non-benzenoid rings will be mentioned in the following sections.

In the case of all-carbon bilayer NGs, they have shown to significantly change their electronic properties depending on the interplanar distance and rotation angle of the NGs. Martín and co-workers reported, at the beginning of 2018, an all-carbon fully fused bilayer NGs with a central [10]helicene,[78] and it was later in 2023 when they presented the synthesis and full chiroptical characterization including CPL of three

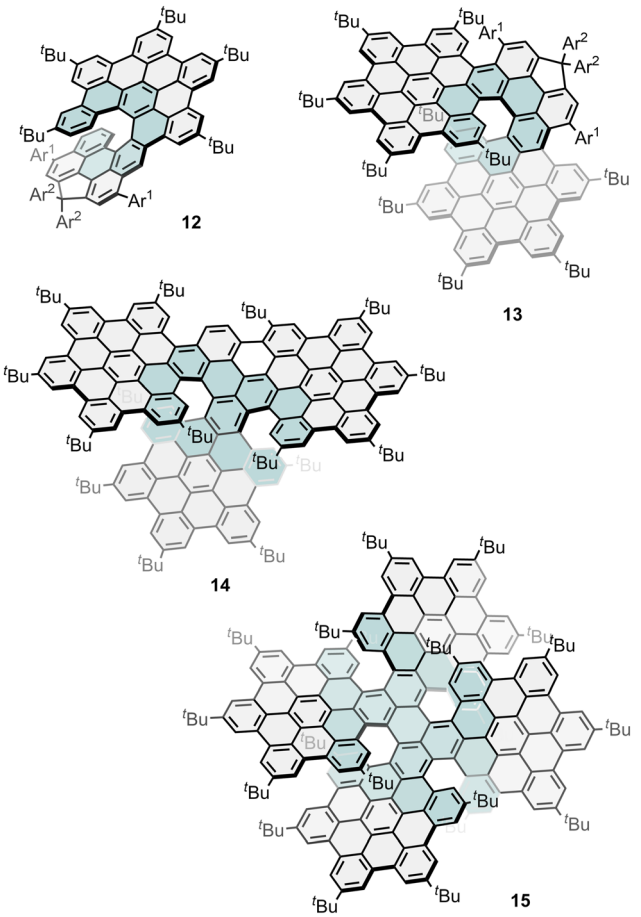

Fig. 5 Examples of chiral perylene-cored nanographenes. Ar^1 = (4-*tert*-butyl)phenyl; Ar^2 = (3,5-di-*tert*-butyl)phenyl.

derivatives constituted by two HBCs linked by a [9], [10] or [11]helicene (**17**, **18**, and **19**, Fig. 6).[79] Ma, Feng and co-workers complemented this family with the [7]helicene analogue (**16**, Fig. 6).[80] Curiously, in this family, the larger conjugation (from [9] to [11]helicene) resulted in a hypsochromic shift of the emission (λ_{em} = 575, 543 and 528 nm, respectively) and in a decrease in both the dissymmetry factor ($|g_{lum}|$ = 3.6 × 10^{-2}, 1.0 × 10^{-2} and 0.9 × 10^{-2}, respectively) and the intensity (Φ_F = 0.22, 0.10 and 0.11, respectively) of the emission. A careful structural comparison of this family showed that the size of the carbohelicene link has great impact on the overlapping of the bilayer π-system, being maximized in **17**, with the shorter carbo[9]helicene. In a related example, Aratani and co-workers reported in 2021 a bilayer compound by bridging two coronenes with a 1,8-naphthalene hinge.[81] X-Ray crystallographic analysis revealed that the *anti*-form is a chiral twisted bilayer coronene type, with an internal bilayer distance of 2.914 Å. Therefore, it was optically resolved and characterized by ECD and CPL spectroscopy. The absolute dissymmetry factor values were moderate reaching 1.5 × 10^{-3} for $|g_{abs}|$ at 436 nm and 2.0 × 10^{-3} for $|g_{lum}|$ at 435 nm.

Ma, Feng and co-workers have presented a modular synthetic strategy to construct a series of multilayered helical NGs

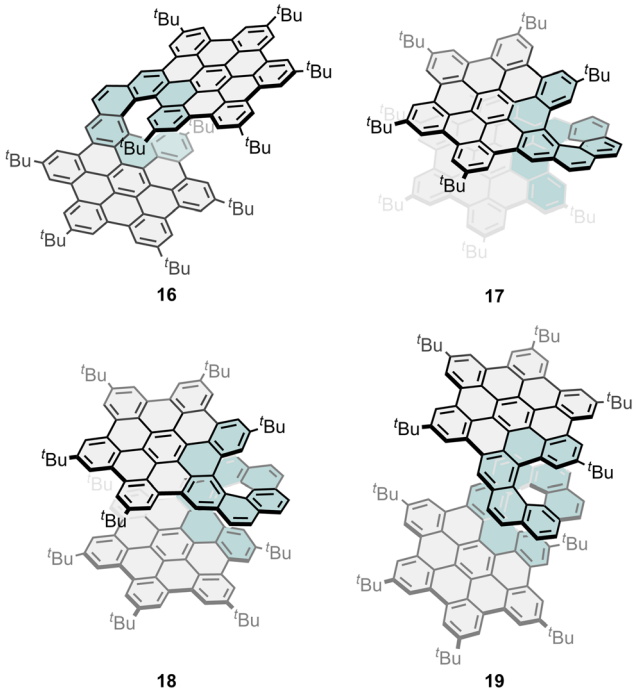

Fig. 6 Examples of bilayer nanographenes connecting two HBC units through a [7], [9], [10] and [11]helicene.

(**16**, **20**, and **21**, Fig. 6 and 7) through a consecutive Diels–Alder reaction and regioselective cyclodehydrogenation from phenanthrene-based precursors substituted with ethynyl groups.[80] In this report, they highlighted the change in the photophysical properties of these helical NGs with respect to the degree of π-extension, which varies with the number of layers, leading to obvious redshifted absorption, a fast-rising ε, and markedly boosted Φ_F. Moreover, the embedded [7]helicene subunits in these NGs result in configurational stability, enabling both chiral resolution and exploration of their layer-dependent chiroptical properties. For that, they investigated the CPL spectra of the isolated enantiomers of **16**, **20** and **21**. Every pair of NG enantiomers showed mirror-like CPL spectra, revealing a gradually declined $|g_{lum}|$ of 7.9×10^{-3} for **16** at 563 nm, 2.7×10^{-3} for **20** at 575 nm, and 1.5×10^{-3} for **21** at 595 nm, respectively, despite the increased number of helicenes and larger conjugation. These trends closely aligned with the observed tendency of $|g_{abs}|_{max}$ which also decreased in the larger analogues. These results again show that increasing the structural complexity and number of helicenes does not always result in improved chiroptical response. Despite the modest $|g_{lum}|$ values found for these layered NGs, the intense ε and high Φ_F ensure high B_{CPL}, whose values were estimated as 168, 112, and 106 M^{-1} cm^{-1} for multilayer NGs **16**, **20** and **21**, respectively. In a subsequent study, Ma, Niu and co-workers also reported the influence of the geometric arrangement of three units of HBC linked by double [7]helicenes. To this end, they compared the chiroptical response of above-mentioned compound **20** (Fig. 6), where the two [7]helicene units are fused at the *ortho* position of the central HBC moiety with two other analogues that are linked in the *para*- (**22**, Fig. 7) and *meta*-position (**23**, Fig. 7).[82] To explain the changes in dissymmetry factors and establish the relationship between the geometry of double [7]helicenes and their chiroptical properties, TD-DFT calculations were performed to check μ and m. In the geometric engineering of two [7]helicene units from *ortho*-, *meta*- to *para*-positions, in this order, the θ and $|\mu|$ gradually decrease, while $|m|$ remains at a constant level. This leads to a simultaneous

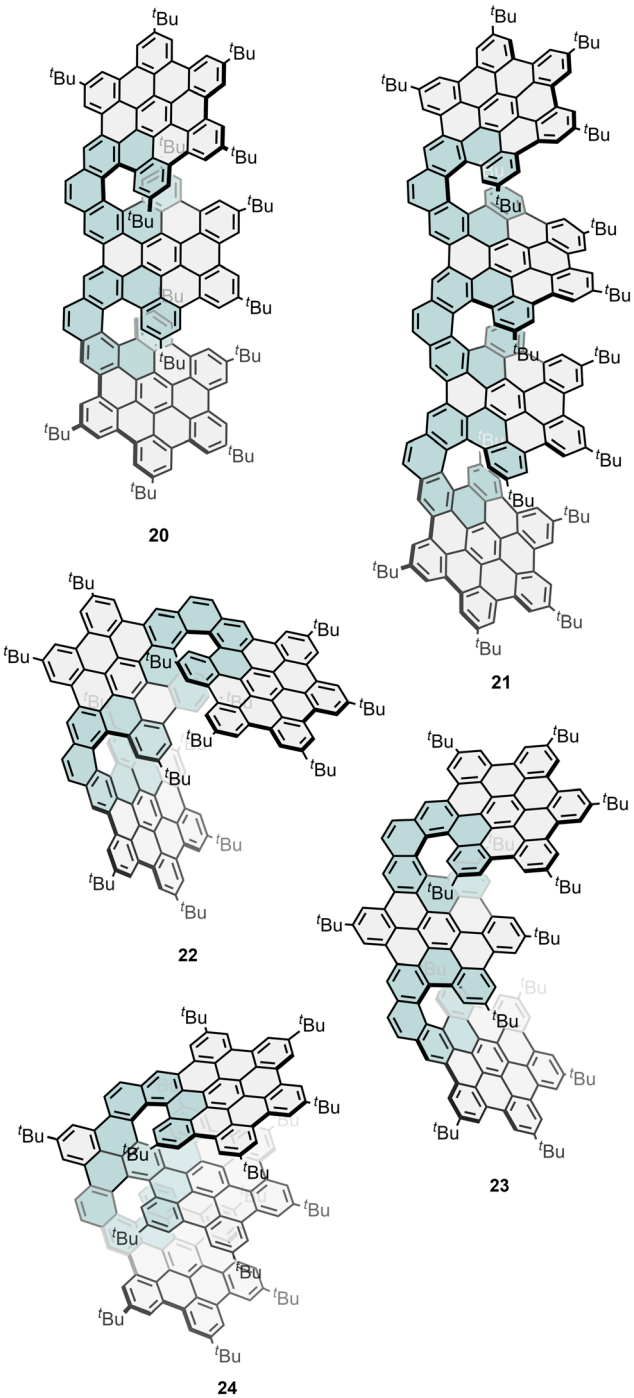

Fig. 7 Examples of multilayer nanographenes connecting three and four HBC units.

increase in $\cos\theta$ and $|m|/|\mu|$, consequently resulting in a significant boost of $|g_{abs}|$ of 3.9×10^{-3} for **20**, 10×10^{-3} for **22** and 18×10^{-3} for **23**. Continuing, they did TD-DFT calculations on their excited state to understand the origin of the increased g_{lum} values. A comparison with **20** reveals a simultaneous increase in $\cos\theta$ and $|m|/|\mu|$ for **22** and **23**, resulting in increased g_{lum} values of 2.7×10^{-3} for **20**, 8.7×10^{-3} for **23**, and 13.5×10^{-3} for **22** together with B_{CPL} values of 112, 143 and 176 M^{-1} cm^{-1}, respectively. Tan and co-workers reported another trilayer NG (**24**, Fig. 7) with a double helicene, together with its O-doped analogue (see Section 2.4.4).[83] The two enantiomers of **24** showed a series of mirror-image Cotton effects extending to 610 nm, indicating a chirality transfer throughout the molecule and showing a maximum $|g_{abs}|$ of 4.2×10^{-3} at 472 nm and a $|g_{lum}|$ value of approximately 1×10^{-3}. Related to **24**, Shen and co-workers reported a flag-hinge-like NG with a central peropyrene unit and two lateral HBCs.[84] This NG exhibited a $|g_{lum}| = 5.0 \times 10^{-3}$ with an excellent B_{CPL} of 305 M^{-1} cm^{-1} thanks to its good Φ_F of 0.52.

As mentioned at the beginning of the section, together with the synthesis of *seco*-HBC **1**, the group of Tanaka reported chiral NGs bearing longer π-extended carbohelicenes.[65] They reported the enantioselective synthesis (up to 87 : 13 enantiomeric ratio) of partially π-extended carbo[11] (**25**, Fig. 8) and carbo[13]helicene (**26**, Fig. 8) finding them to be good CPL emitters with $|g_{lum}|$ values of 4.0×10^{-2} and 3.4×10^{-2} and a very high B_{CPL} of 490 and 287 M^{-1} cm^{-1}, respectively. These π-extended helicenes are synthesized *via* an enantioselective triple [2+2+2] cycloaddition to construct low-distortion expanded carbo[13] and carbo[15]helicene skeletons, followed by subsequent π-extension by means of the Scholl reaction.

These last examples show structures where the HBC units are linked through [*n*]helicenes. However, HBC moieties can be arranged to create fully extended [*n*]helicenes. Thus, the simplest example could be the arrangement of two HBCs into an extended carbo[5]helicene, however, this structure remains unexplored and only a heptagon-containing analogue has been reported by our group (Section 2.3.2, Fig. 12, compound **38**). Conversely, its double carbo[5]helicene analogue has been reported by Wang and co-workers,[85] however, its chiroptical properties remain unexplored. Other impressive examples with even larger structures, bearing multiple helical motifs have been reported by the same group.[86,87] Nevertheless, CPL was not determined for any of these compounds. Regarding this family (often called superhelicenes), a ribbon-shaped NG constituted by four HBC units arranged around a central fully π-extended carbo[9]helicene was presented by Gong and co-workers in 2024 (**27**, Fig. 9).[88] The large conjugated framework resulted in an emission in the NIR (600–900 nm) and the helical shaped resulted in a considerable $|g_{lum}|$ value of 4.50×10^{-2}, and a B_{CPL} as large as 304 M^{-1} cm^{-1}, both higher than the values reported for bilayer **17** bearing a central carbo[9]helicene moiety as well. Those results aim again to the lateral π-extension and elongation of chiral NG to enhance their emissive and chiroptical properties. The same group reported two analogues of **27** containing pore defects at one or the two edge HBC units.[89] Remarkably, these pore-containing analogues exhibited lower $|g_{abs}|$ and $|g_{lum}|$ than **27** in solution. Additionally, in polymethyl methacrylate (PMMA) and powder films, both analogues show lower $|g_{abs}|$ and $|g_{lum}|$. The presence of these pore defects led to a blue shift in the ECD and CPL spectra. Later, the same group presented a larger example constituted by five HBC units arranged in a W-shape bearing two fully π-extended [7]helicenes (**28**, Fig. 9) displaying fluorescence emission (λ_{em} = 636 nm) with a $\Phi_F = 0.10$.[90] In this case, despite the larger π-system, it exhibits lower $|g_{lum}|$ of 4×10^{-3}, and a B_{CPL} of 42 M^{-1} cm^{-1} in one order of magnitude compared with the previous smaller member of the family, pointing out the importance of the mutual arrangement when two carbohelicenes are present. Single crystals of **28** revealed that the racemic mixture crystallizes in the triclinic $P\bar{1}$ space group, with each enantiomer featuring two identical carbo[7]helicene units. The enantiomers pair into dimers, stabilized by π–π and CH–π interactions between neighboring HBC units. These dimers self-assemble into a one-dimensional architecture, extending to a three-dimensional network *via* CH–π interactions, showcasing a remarkable hierarchical organization (Fig. 9).

Another example of a compound bearing double π-extended helicenes was reported by Hu, Narita and co-workers, which presented a π-extended double [9]helicene with remarkable NIR emission. However, they did not report its CPL response, whereas its side product (**29**, Fig. 9) shows a $|g_{abs}|$ value of 0.008 at 582 nm. In addition, the CPL of **29** was also measured, showing a $|g_{lum}|$ of 4×10^{-3}.[91]

Recently, Ravat and co-workers reported helically twisted chiral nanoribbons featuring a central pyrene core, or fused pyrenes, anchored at the terminal K regions through one or two [7]helicenes (compounds **30–33** Fig. 10) *via* stereospecific APEX reactions.[92,93] The [7]helicene influences on the conformational stabilization according to the DFT and single crystal structure analyses. The experimentally obtained $|g_{lum}|$ of **30** and **31** is 1.27×10^{-3} and 0.63×10^{-3}, respectively, evidencing the negative effect of fusing additional pyrene units. Conversely, the $|g_{lum}|$ of **32** and **33** were evaluated as 0.54×10^{-3} and 1.54×10^{-3}, respectively, which points to the additional [7]helicene as a key factor to enhance the CPL response. This fact was further supported by TD-DFT, which

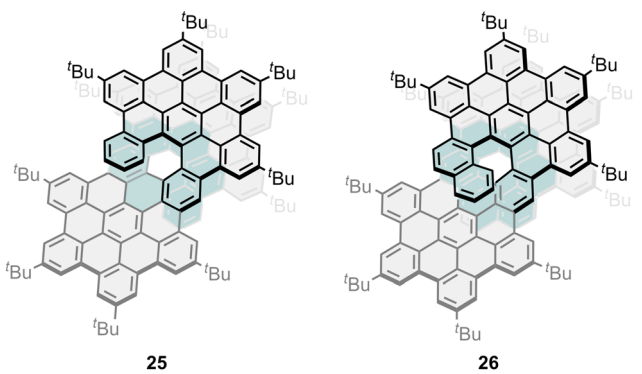

Fig. 8 Examples of *seco*-HBC arranged around a central helicene reported by Tanaka and co-workers.

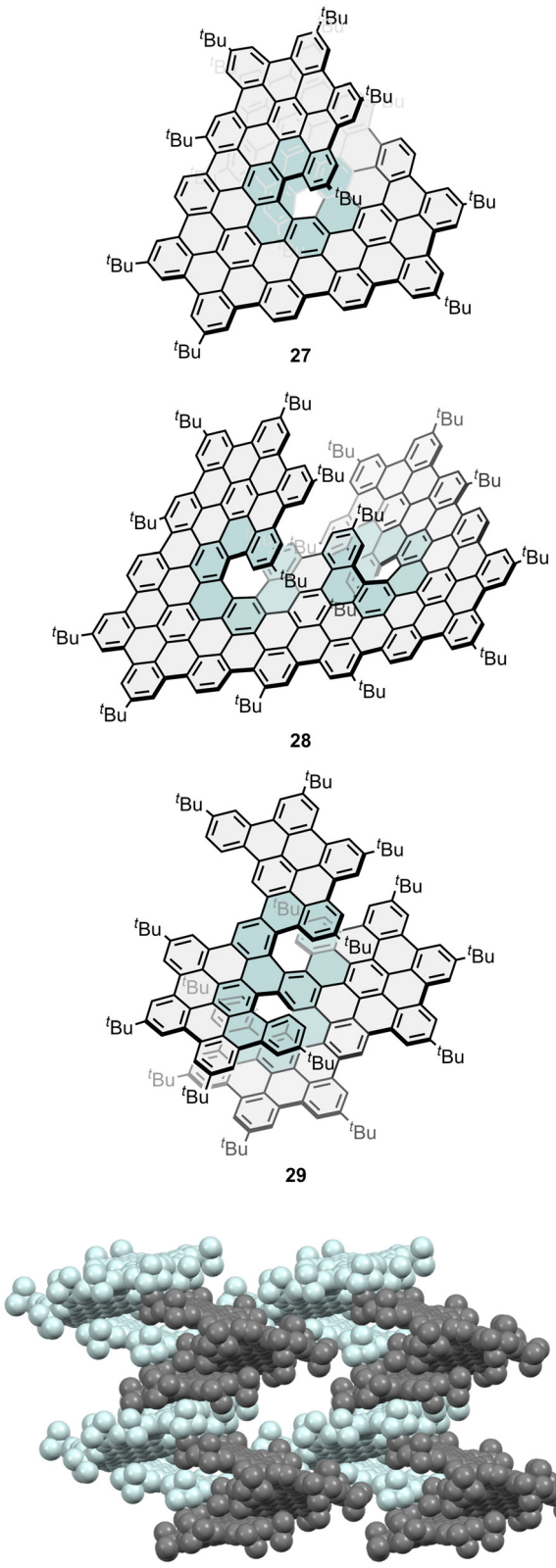

Fig. 9 Examples of nanographenes as fused HBC units arranged around [*n*]helicenes. Crystal packing of **28** (bottom).

predicted a larger $|m|$ and higher $\cos\theta$ values for the $S_1 \rightarrow S_0$ transition in **33** compared to those in **32** and **30**.

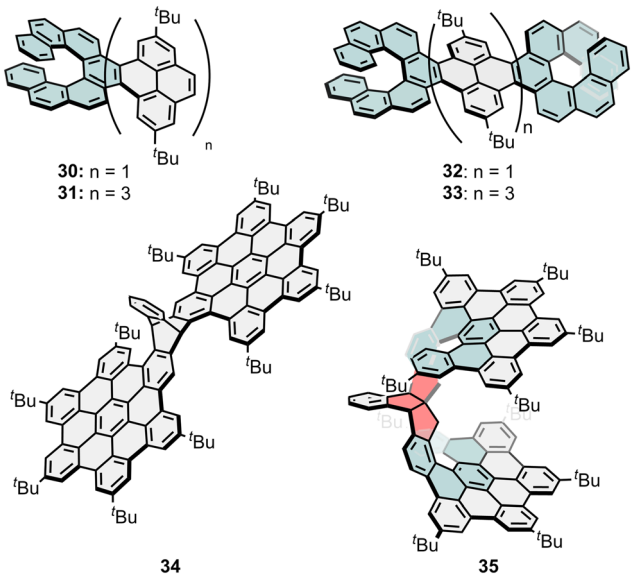

Fig. 10 Chiral nanographenes combining helicene(s) and pyrene units (**30–33**), triptycene-fused double HBC-based nanographene (**34**) and triindane-fused double seco-HBC nanographene (**35**) as CPL emitters.

In addition to the inclusion of helicenes as intrinsic chirality providers in NGs, less common chiral scaffolds bearing asymmetric carbon atoms are also of great interest. Such is the case of triptycene, which has been used as efficient solubilizing group of large PAHs,[94] three-dimensional scaffold,[95,96] and can also bridge two HBC units to create a chiral NG as shown by Ikay group (**34**, Fig. 10).[97] In this case, the chirality is provided by the two asymmetric sp^3 carbon atoms present in the triptycene moiety. Its forbidden conformational interconversion allowed its resolution by HPLC, as well as the crystallization of one of the enantiomers, after which the evaluation of the CPL resulted in $|g_{lum}|$ values of 1.0×10^{-3}. Another interesting example is the triindane moiety, which has been used by Martín and co-workers as a chiral linker between two *seco*-HBC (**35**, Fig. 10).[98] The synthesis of **35** is performed through an enantiospecific Scholl reaction, with the triindane acting as chiral auxiliary unit. Compound **35** possess three asymmetric carbon atoms and two carbo[5]helicenes, being possible to conduct its racemic resolution. CPL response of **35** was evaluated with a $|g_{lum}| = 1.9 \times 10^{-3}$ and a $B_{CPL} = 16.7\ M^{-1}\ cm^{-1}$. Despite the generalized lack of asymmetric sp^3 carbon atoms in extended polycyclic conjugated hydrocarbons (PCHs) and NGs, it is possible to find new CPL-active carbon-based structures containing tetragonal stereogenic centres, which originates novel architectures from interesting scaffolds. Recently, Du and co-workers reported a cycloparaphenylene-HBC (CPP-HBC) hybrid as CPL emitter.[99] The synthesis was based on the preparation of a cycloparaphenylene unit functionalized with two triflate moieties over the same benzene ring. Thus, a further Suzuki coupling with two equivalents of a boronic ester HBC derivative yielded the target NG. The corresponding enantiomers were separated by chiral stationary phase HPLC, where the size of the HBCs prevented its racemization. This CPP-HBC hybrid

showed Φ_F = 0.35 with a CPL centred at 469 nm with $|g_{lum}|$ = 1.10 × 10^{-3}.

2.3. NGs bearing non-benzenoid rings

As mentioned in Section 2.2, inducing chirality in NGs is mainly tackled by attaching inherently chiral motifs within the π-conjugated scaffold. Helicenes are one of the most commonly implemented chiral elements since they are complemented by a delocalized electronic structure. The combination of helicenes and non-benzenoid rings is a recurrent strategy to alter both the distortion and chiroptical properties of NGs. Therefore, this section covers those NGs bearing non-benzenoid rings in their structure and displaying CPL. Introduction of non-benzenoid rings with different sizes can generate many types of curvatures, for example, including pentagonal rings in the π-conjugated core generates a positive curvature while insertion of heptagonal rings generates a negative curvature, both having an influence in the (chir)optical properties of the resulting molecules. Thus, reported examples of NGs containing five-, seven-, eight- and nine-membered rings, where the helicene insertion strategy is used, are reviewed in this section. This section is organized according to the sizes of the non-benzenoid ring and, specifically the seven-membered ring section, according to the location of this non-benzenoid ring (either in the chiral unit, in the helicene, or in the NG core).

2.3.1. Five-membered rings. Two examples of NGs bearing five-membered rings as CPL emitters have been reported to date. In 2021, Jiang and co-workers developed two chiral NGs based on a corannulene unit. One featuring a [4]helicene and another one comprising a [7]helicene (**36**, Fig. 11).[100] For the [4]helicene analogue the racemisation barrier at room temperature was too low (4.7 kcal mol^{-1}) to perform a racemic resolution, thus, the authors were unable to obtain enantiopure samples. In contrast, for **36**, which exhibited a λ_{em} centred at 508 nm and Φ_F = 0.22 in a $CHCl_3$ solution, the CPL response was evaluated, obtaining a $|g_{lum}|$ value of 0.43 × 10^{-3}. A π-expanded X-type double [5]helicene comprising two dihydropyracylene moieties was synthesised by Kivala and co-workers (**37**, Fig. 11).[101] Compound **37** exhibited a λ_{em} centred at 569 nm and Φ_F = 0.43. After the racemic resolution of both enantiomers, the CPL was evaluated, showing $|g_{lum}|$ values of about 1 × 10^{-3}.

2.3.2. Seven-membered rings. NGs bearing heptagonal rings have been synthesized by either embedding the seven-membered ring as part of a helicene subunit or not. Thus, back in 2018, our group reported the first example of a NG with CPL emission with the synthesis of a ribbon-shaped helical NG (**38**, Fig. 12) bearing two HBC units fused by an extended [5]helicene and with a heptagonal ring at the edge of the structure.[51] The structure was confirmed by single crystal X-ray crystallography. In the crystal, **38** appears as a pair of enantiomers, forming π-stacked dimers with a π–π distance of 3.4–3.5 Å. Within each dimer, the molecules adopt an antiparallel arrangement,

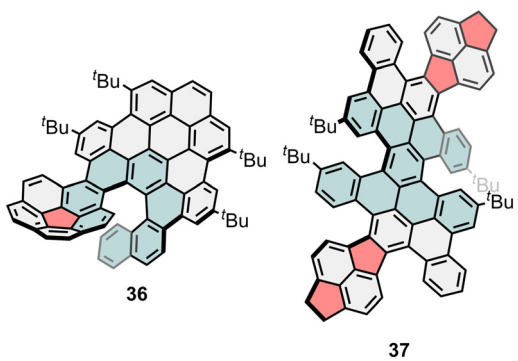

Fig. 11 Chiral nanographenes showing exhibiting a corannulene moiety (**36**) and two pyracylene moieties (**37**) as five-membered ring containing CPL-active nanographenes.

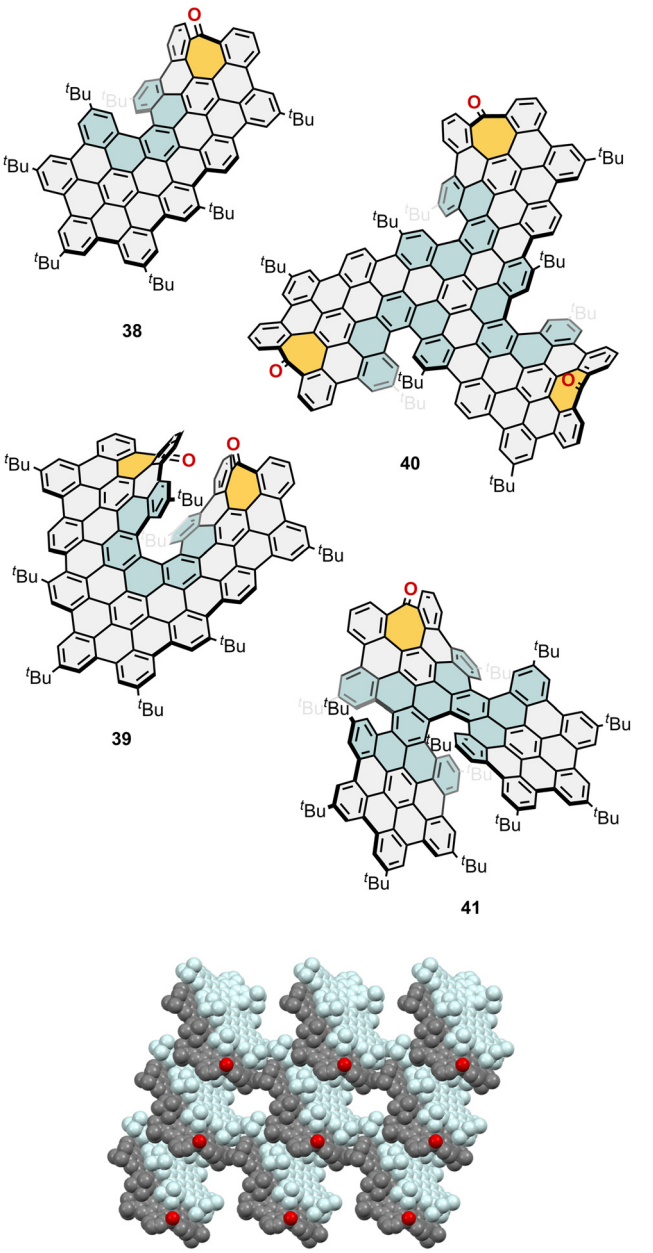

Fig. 12 Saddle-helix hybrid nanographenes with CPL response, prepared by Campaña and co-workers. Crystal packing of **38** (bottom).

interacting through the planar regions on the non-defective side (Fig. 12). The CPL spectra showed an emission maxima centred at 560 nm and the $|g_{lum}|$ value was evaluated as 0.23×10^{-3}. The same year, we also presented a chiral helical NG with an extended [7]helicene, an undecabenzo[7]helicene, and containing two heptagonal rings (**39**, Fig. 12).[53] This was the first fully helical ribbon with a π-extended central carbohelicene exhibiting CPL response. Mirror image CPL spectra centred at 610 nm were obtained for both enantiomeric forms of **39**, and the $|g_{lum}|$ reached a value of 2×10^{-3}, which represents a significant one order of magnitude increase in comparison with **38**. During the following years, our group presented several members of this saddle-helix hybrid NG family by embedding seven-membered rings within the conjugated scaffold, such as the triskelion-shaped saddle-helix hybrid NG reported in 2019 (**40**, Fig. 12).[102] Compound **40** was synthesized with an increased number of embedded heptagonal rings compared to **38** and **39**, and also three extended [5]helicenes. Therefore, it was obtained as a mixture of two diastereomers, a C_3-symmetric (*P*,*P*,*P*/*M*,*M*,*M*)-**40** and a C_1-symmetric (*P*,*P*,*M*/*M*,*M*,*P*)-**40**. For the former, the CPL spectra show a maximum centred at 643 nm and an estimated $|g_{lum}|$ value of 0.3×10^{-3}, whilst for the enantiomeric forms of the latter, the maximum is located at 656 nm with a $|g_{lum}|$ value of 0.2×10^{-3}. We also carried out a study in 2020 in which we could shed light on the insertion effect of these non-benzenoid rings,[103] specifically heptagonal rings. In 2022, our group presented another highly contorted superhelicene (**41**, Fig. 12) as well.[104] Compound **41** was designed to improve the Φ_F, to reveal the influence of the tropone position, and the addition of multiple carbohelicenes in the structure of **39**. Surprisingly, the absorption and emission spectra were redshifted by nearly 100 nm in **41**. Two enantiomers were isolated, (*P*,*P*,*M*/*M*,*M*,*P*)-**41**, both showing CPL response and exhibiting $|g_{lum}|$ values of 3×10^{-3}. Additionally, the CPL response was evaluated in thin films of **41**, obtaining opposite CPL spectra for both enantiomers. Regarding NGs featuring seven-membered rings embedded into the structure of the helicene, Xiao and co-workers described the synthesis of a heptagon-embedded helical arene (**42**, Fig. 13).[105] Compound **42** exhibited a fluorescence spectrum centred at 537 nm with $\Phi_F = 0.02$. The enantiomers of **42** were separated and the evaluated g_{lum} reached values of -1.1×10^{-3} for (*P*)-**42** at 503 nm. These g_{lum} values are similar to those reported by Ravat and co-workers for a pyrene analogue.[92] In 2024, Kivala and co-workers reported the CPL response of one of the intermediates obtained during the synthesis of π-expanded azocines.[106] This compound (**43**, Fig. 13), containing a heptagon-pentagon pair, showed an emission maximum at 542 nm and a remarkable $\Phi_F = 0.47$. Enantiopure forms of **43** exhibited $|g_{lum}|$ values of 0.94×10^{-3}, lower than its related azocines that will be discussed in the following section. As a last example, Feng and co-workers developed a helical bilayer non-benzenoid NG bearing a [10]helicene with two embedded heptagons, one of them as part of an azulene moiety (**44**, Fig. 13).[107] Its emission maximum was found at 602 nm with a low Φ_F value of 0.0032. The $|g_{lum}|$ reaches up to 1.3×10^{-3}, within the range of the previously mentioned heptagon-embedded helical NGs.

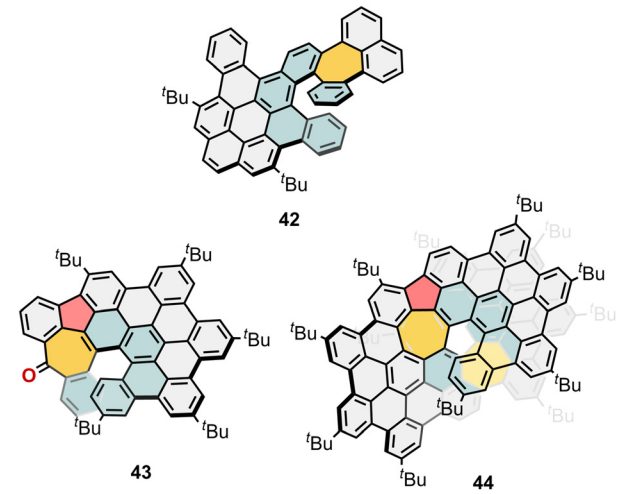

Fig. 13 Chiral nanographenes exhibiting heptagons as part of the helicene moiety.

2.3.3. Eight- and nine-membered rings. Interesting structures of octagon-containing NGs can be found in literature.[108] Chiral counterparts, such as the four-fold HBC arranged around a central cyclooctatetraene unit, have been reported by Martín and co-workers.[109] However, in most cases, their CPL spectra are not available. The first examples of CPL-active NGs containing eight-membered rings were reported in 2021 in our research group.[110] Therein, a new family of saddle-helix hybrid NGs with octagonal rings was synthesized. In this family, **45** and **46** (Fig. 14), the octagonal ring was embedded into both the HBC and the carbohelicene moieties. For **45**, the CPL spectra showed a maximum centred at 470 nm and an estimated $|g_{lum}|$ value of 0.4×10^{-3}, whilst $|g_{lum}|$ values of 0.7×10^{-3} at 554 nm for **46** were determined. In 2021, we also attempted to measure CPL responses of a nonagon-embedded NG family.[111] As a selected example, the nonagon-containing a [5]helicene (**47**, Fig. 14), obtained from a ring expansion of **45**, resulted in an extremely twisted helical moiety. This combination of structural features provided **47** with enhanced chiroptical properties in the absorption (more than two-fold compared to **45** and **46**). However, emission profiles of this family were non-trivial as fluorescence measurements revealed

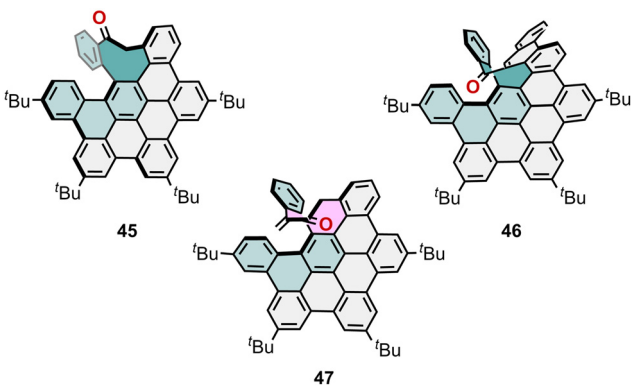

Fig. 14 Saddle-helix hybrid nanographenes exhibiting an octagon (**45** and **46**) and nonagon (**47**) ring, prepared by Campaña and co-workers.

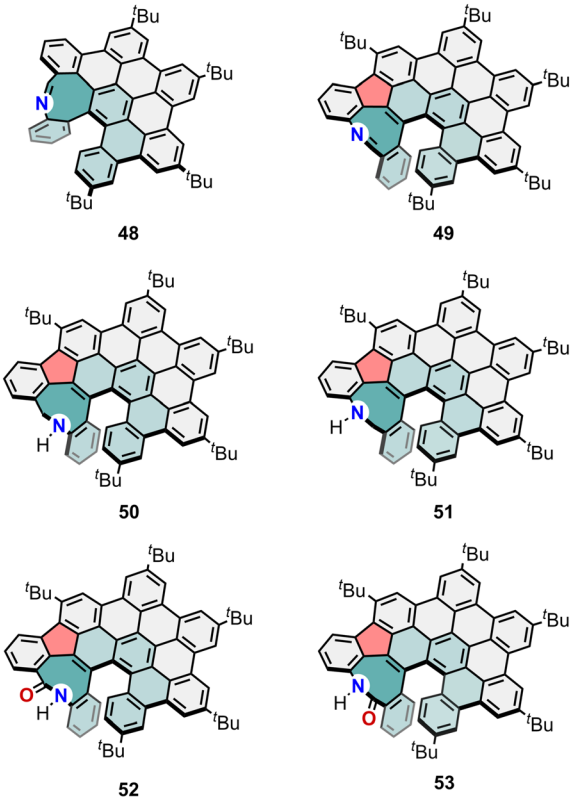

Fig. 15 CPL-active nanographenes containing an azocine moiety (**48** and **49**) and related amines and lactams (**50–53**).

changes in the emission profiles under the long-time irradiation required for CPL measurements.

In view of the above-presented results, introducing non-benzenoid rings in the NG scaffolds evidences a great influence in the structure of the resulting NG. It enhances racemization barriers and improves configurational stability, avoiding the use of bulky substituents in the fjord region. Therefore, it leads to a higher distortion when embedded into the structure of a helicene compared to its fully hexagonal analogue.

2.4. NGs bearing heteroatoms

2.4.1. Nitrogen-doped chiral NGs. NGs exhibiting CPL and bearing N-doped octagonal rings will be firstly revisited in this section. Both, our and Kivala's group have developed azocine-containing NGs exhibiting CPL. In 2021, an azocine-embedded HBC analogue was synthesized by An and co-workers.[112] Then, it was in 2023, when our group prepared an azocine-embedded HBC bearing *tert*-butyl substituents (**48**, Fig. 15).[113] This N-doped NG provides additional chemical stability with regards to the evaluation of its chiroptical properties, in comparison with its carbon-based analogue,[110] and the possibility to modulate the ECD and CPL signals with external stimuli, such as redox or pH changes. The reversibility of this switching was also confirmed. Chemical and electrochemical oxidation of **48** suggest that the produced radical and a radical-cation species centred into the N atom could modulate the chiroptical response, due to the appearance of new bands in the NIR-region of the ECD spectra. On the other hand, we inferred the same conclusion with the protonated/neutral species, highlighting that CPL emission can be switched off/on with different acid–base additions. The CPL spectra of **48** showed a maximum centred at 457 nm with a $|g_{lum}|$ value of 0.8×10^{-3} and a B_{CPL} of 1.40 M^{-1} cm^{-1}. A related family was presented in 2024 by Kivala group with a series of multiple N-doped NGs bearing N-containing octagonal rings fused with pentagonal rings.[106] Amines **50** and **51** (Fig. 15), and lactams **52** and **53** (Fig. 15) showed CPL with similar g_{lum} values ranging from 0.91×10^{-3} to 0.24×10^{-3}. In the case of imine **49** (Fig. 15), a further increase of the $|g_{lum}|$ value up to 1.6×10^{-3} was found. According with a thorough theoretical analysis, they understood the influence of the azocine and the indene moieties in the properties, highlighting the evolution in the aromaticity of the azocine after reduction/oxidation cycles, suggesting that the steric hindrance blocks the aromatization of the azocine unit. To conclude, they report that the indene unit is accountable for the redox chemistry of the species, whereas changes in azocine unit are insignificant.

In 2023, Qiu and co-workers reported a curved NG bearing a [1,4]diazocine and octagon-pentagon fused rings (**54**, Fig. 16) reaching a g_{lum} value of 0.26×10^{-3} for (*P*)-**54** at λ_{em} = 450 nm.[114] The g_{lum} values were reported in solution, in contrast to their aggregates, which resulted to be CPL-silent. Despite that, in aggregate state these species can form a charge transfer complex with non-chiral acceptors, such as tetrafluoroterephthalonitrile (TFTPM) and 1,2,4,5-tetracyanobenzene (TCNB), and activate the CPL response. The former showed yellow emission reaching g_{lum} values of $+0.41 \times 10^{-3}$ for (*M*)-**54**:TFTPM at 587 nm. The latter showed red emission reaching g_{lum} values of -1.4×10^{-3} for (*P*)-**54**:TCNB at 655 nm. The same group reported another related analogue based on a carbazole-built π-extended diaza[7]helicene with double negatively curved heptagons generated by Pd-catalysed intramolecular C–H arylations (**55**, Fig. 16).[115] Compound **55** exhibited intense green fluorescence with λ_{em} = 517 nm and their enantiopure samples showed a bisignated CPL spectra with $g_{lum} = 2.0 \times 10^{-3}$ at 545 nm.

Recently, Casado, Liu and co-workers presented the development of a non-alternant NG containing a N-centred cyclopenta[*ef*]heptalene and an aza[7]helicene units.[116] These strained moieties represent a heteroatom-doped member of the saddle-helix hybrid NG family with CPL response. Compounds **56** and **57** (Fig. 16) were synthesised to evaluate the relevance of the π-extension of the cyclopenta[*ef*]heptalene in the chiroptical properties of the helical NGs. Single crystal structure of **57** show multiple CH–π contacts allowing the formation of 1D columns with close packing (Fig. 17). They reported $|g_{lum}|$ values of 7.0×10^{-3} for **57** that are significantly larger than the $|g_{lum}|$ values for the non-extended one (**56**, $|g_{lum}| = 2.4 \times 10^{-3}$). These compounds also showed intense fluorescence and phosphorescence emission, specifically, **57** showed a narrow red emission centred at 588 nm with a Φ_F = 0.32. Two new carbazole-centred extended helically NGs, (**58** and **59**, Fig. 16), were reported by the groups of Babu and Gong, respectively.[117,118] The structural difference between compounds **58** and **59** lies in the substituent of the

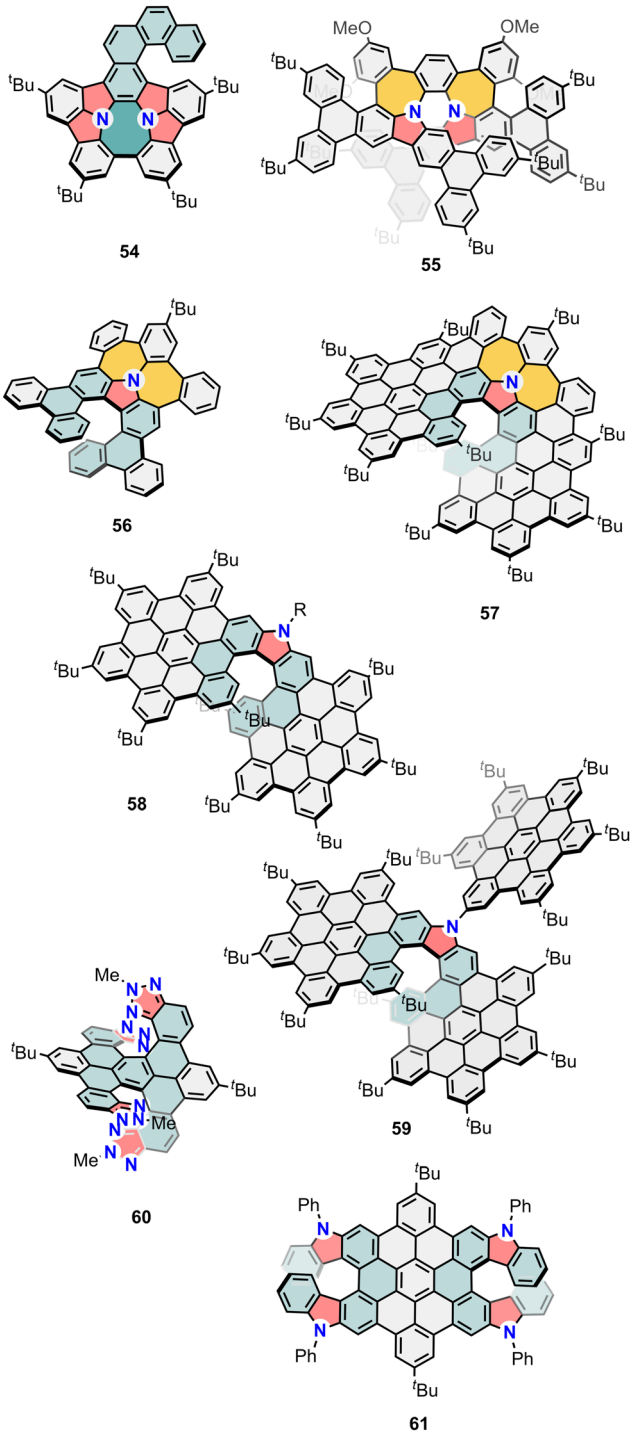

Fig. 16 N-doped chiral nanographenes exhibiting CPL response. Nanographenes. R = hexyl.

carbazole moiety, bearing a hexyl or HBC unit, respectively. These compounds exhibit an orange/red fluorescence in solution (λ_{em} = 542 and 595 nm for **58** and **59**, respectively) with a high Φ_F of 0.75 and 0.40. The substitution of the carbazole unit by incorporation of an hexyl or HBC units affords additional chemical and configurational stability, compared to the unsubstituted one, reported by Jux and co-workers.[119] In the study of

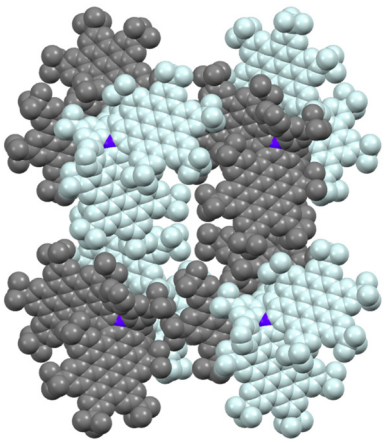

Fig. 17 Unit cell showing the crystal packing in compound **57**.

59, the authors observed that the B_{CPL} depends on the solvent, achieving a lower value in CH_2Cl_2 (g_{lum} = 0.43 × 10^{-3} for (*P*)-enantiomer and B_{CPL} = 9.89 M^{-1} cm^{-1}). While solutions in THF (g_{lum} = 1.06 × 10^{-3} and B_{CPL} = 28.57 M^{-1} cm^{-1}) and MeCN (g_{lum} = 1.30 × 10^{-3} and B_{CPL} = 19.43 M^{-1} cm^{-1}) exhibited higher g_{lum} and B_{CPL} values. On the other hand, the $|g_{lum}|$ for compound **58** in 2-methyl-THF was evaluated as 1.1 × 10^{-3}, reaching a B_{CPL} of 45.77 M^{-1} cm^{-1} for (*M*)-**58**.

Hu and co-workers reported a double hetero[7]helicene fused with four triazole rings (**60**, Fig. 16) in 2022.[120] The N-doping proved to have a great impact on the luminescence intensity, reaching a Φ_F = 0.96 as well as in the g_{lum}, which was significantly enhanced in almost one order of magnitude with respect to its full-carbon analogue (Section 2.2, Fig. 3, compound **6**) reaching a value of 9.1 × 10^{-4} for (*P*,*P*)-**60**. The terminal triazole units provide the compound with an ambipolar redox behaviour, where stable radical cations were formed by both chemical and electrochemical methods. This double terminal triazole helicenes constitute an interesting platform to modulate emissive, chiroptical and electrochemical properties. The same group also presented a doble diaza[7]helicene (**61**, Fig. 16) as an intermediate in the synthesis of a negatively curved aza-NG bearing two octagonal rings, with $|g_{lum}|$ values of 2.2 × 10^{-3}.[121] Curiously, the final curved saddle-shape NG showed an electron-rich nature that leads to an interesting association with fullerenes (K_a = 9.5 × 10^3 M^{-1} with C_{60} and K_a = 3.7 × 10^4 M^{-1} with C_{70}).

Recently, Babu and co-workers reported the synthesis of a three π-extended helical NG family.[122] These helical NGs are constituted by a phenazine-embedded bilayer NG (**62**, Fig. 18) with $|g_{lum}|$ = 0.73 × 10^{-3}, and two [1,4]-diazocine-embedded helicenes (**63** and **64**, Fig. 18) with $|g_{lum}|$ = 0.89 × 10^{-3} and $|g_{lum}|$ = 5.5 × 10^{-3}, respectively, for the *P*-enantiomers. Specifically, the insertion of a [1,4]-diazocine-helical moiety in **64** shows an enhancement of the chiroptical properties. The incorporation of this helical moiety was useful in engineering θ. In addition, this work shows that the aromaticity character of the diazocine unit takes relevance in the determination of both types of transition dipole moments. Due to the antiaromatic

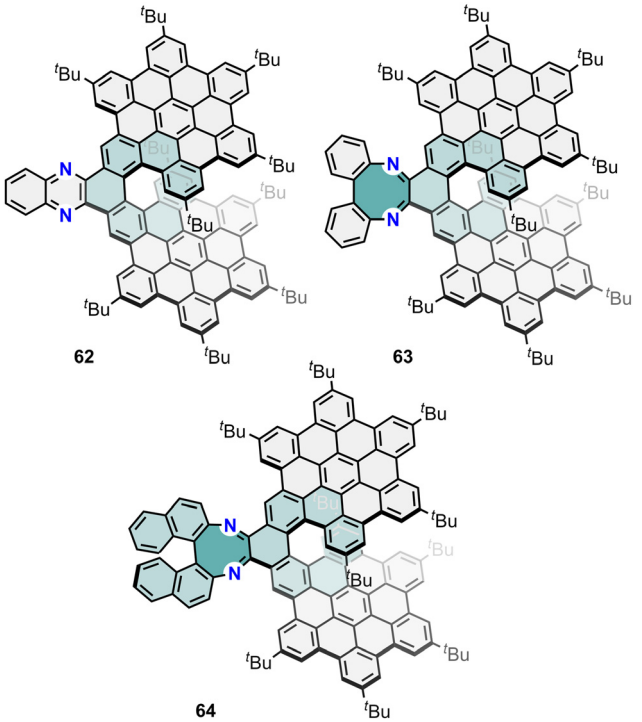

Fig. 18 Phenazine- (**62**) and [1,4]diazocine-embedded (**63** and **64**) bilayer nanographenes reported by Babu and co-workers.

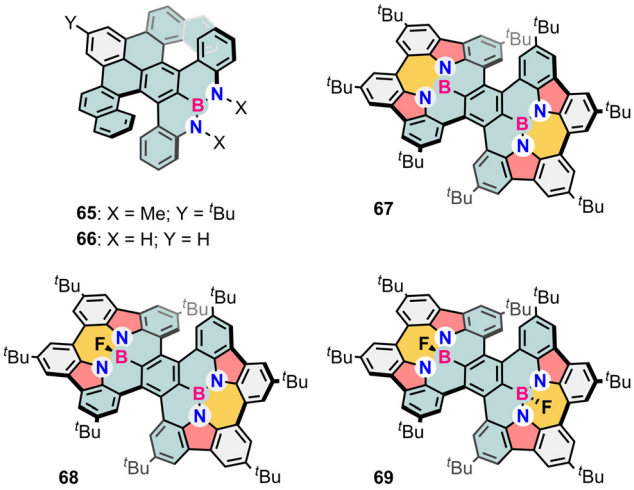

Fig. 19 Chiral B,N-doped nanographenes exhibiting NBN units with reported CPL.

character of the diazocine unit, **63** and **64** show an enhance of their *m* values which contribute to get the $|g_{lum}|$ values of the reported π-extended helical NG **64**. These compounds can be also compared to the bilayer NG **16** (Section 2.2, Fig. 6), to understand the effect of embedding a phenazine or a [1,4]-diazocine into its structure. Remarkably, the pristine bilayer NG **16** exhibited a $|g_{lum}|$ of 7.9×10^{-3}, which represents a higher value compared to **62**, **63** and **64**.

Finally, within the context of N-doped NGs, it should be noted that we have considered chiral perylene diimides (PDIs) or naphthalene diimides (NDIs) reported as CPL emitters as out of the scope of this review centred in NGs, due to their special structures and particularities.[123–127]

2.4.2. Nitrogen–boron-doped chiral NGs. Among the heteroatom-doping strategies, using B–N units has gained considerable attention. The polar B–N unit keeps the structural similarity but alters the molecular polarity respect of the full-carbon analogue.[128] In this field, Zhang *et al.* reported a π-extended C_2-symmetric double NBN-heterohelicene (**65**, Fig. 19) with CPL response.[129] This specie was synthesised by a highly regioselective Scholl reaction. Compound **65** emitted CPL signal with a $|g_{lum}|$ of 0.75×10^{-3} at 546 nm. Later, the same group reported an analogue without substituents in the nitrogen (**66**, Fig. 19).[130] $|g_{lum}|$ values of 1.1×10^{-3} were found at 532 nm for (*P*,*P*)-**66**. Remarkably, compound **66** exhibit strong binding interactions with fluoride anions. This binding causes a red shift in the CPL response with a decrease in the $|g_{lum}|$ value (0.64×10^{-3}). Structurally related, Yang's group synthesised a series of hetero- and heptagon-doped double helicene with two NBN units (**67–69**, Fig. 19).[131] Enantiomers of **67** show mirror-image CPL spectra with $|g_{lum}|$ around 1.0×10^{-3}, which varies with the used organic solvent. The coordination number of boron has shown significant impact in the optoelectronic properties of B-doped PCHs and NGs, therefore it was of marked interest measuring CPL responses of **68** and **69**. Emission maxima of **67** (λ_{em} = 522 nm) is red shifted upon coordination with one fluoride anion (**68**, λ_{em} = 567 nm) and blue shifted upon coordination of a second fluoride anion (**69**, λ_{em} = 541 nm). This red shift is also observed in the CPL spectra of **68** and **69** was observed with $|g_{lum}|$ values of 1.0×10^{-3}. Remarkably, the Φ_F increases in **68** compared to **67** (0.99 and 0.65, respectively), with compound **69** also exhibiting an extraordinary Φ_F = 0.90.

Recently, a family of NGs based on 2,6-bis(3,6-di-*tert*-butyl-9*H*-carbazol-9-yl)boron (D^{t}BuCzB) was reported by Zhang and co-workers.[132] The authors reported the synthesis of five chiral NGs (**70–74**, Fig. 20), which can be divided in two groups: the ones having a double helical motif (**70**, **71** and **72**) and the ones embedding seven-membered rings in its structure (**73** and **74**). All the family shows thermally activated delayed fluorescence (TADF) and the authors highlighted that the presence of heptagonal rings decreased Φ_F. Contrariwise, these heptagonal rings increased the chiroptical response, producing higher $|g_{lum}|$ values (2.9×10^{-3} for **73**, and 5.0×10^{-3} for **74**) with respect to those ones with only double helical motifs (2.5×10^{-3} for **70**, 2.7×10^{-3} for **71**, and 2.7×10^{-3} for **72**). A similar structure, featuring a fused double D^{t}BuCzB has been studied by Wang and co-workers in 2021 (**75–77**, Fig. 20).[133] This family of double hetero[7]helicenes also exhibited TADF, with λ_{em} centred at 660, 684 and 696 nm, respectively, and extraordinary Φ_F of 1.00, 0.99 and 0.90, for **75**, **76** and **77**, respectively. Mirror-image CPL spectra with $|g_{lum}|$ up to 2×10^{-3} for **75**. The B_{CPL} values of **75–77** were determined as 28.5, 37.1, and 40.0 M^{-1} cm^{-1}, respectively. In 2023, Ravat and co-workers also reported the study of two helicene-fused D^{t}BuCzB analogues.[134] However, their π-extended analogues will be discussed in this review (**78–80**, Fig. 21).[135] The authors reported that the rigidification of the NG core with azaborine units led to an ultra-

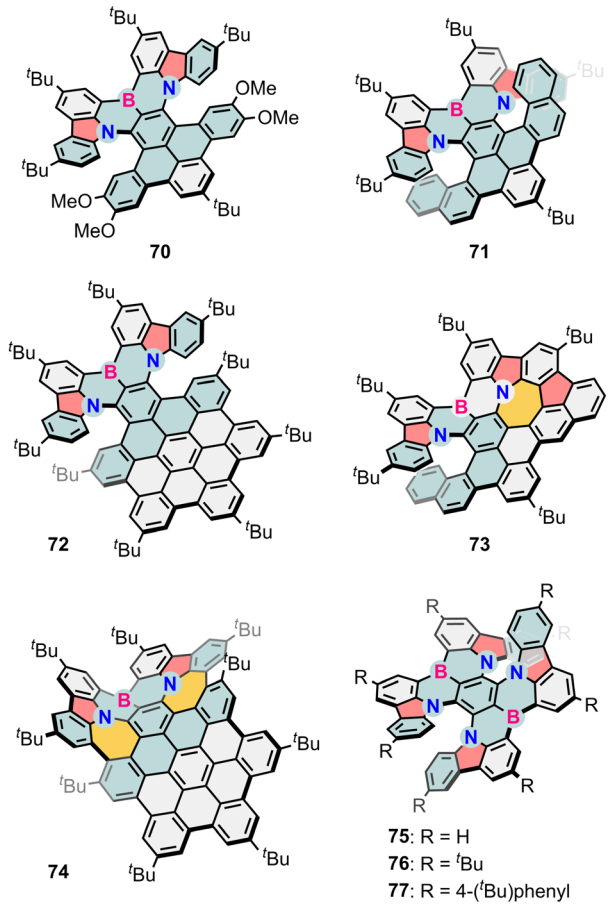

Fig. 20 Chiral nanographenes exhibiting one (**70–74**) or two (**75–77**) units of D^{t}BuCzB.

narrow fluorescence emission, with full width at half maximum (FWHM) of 17.5, 16 and 17 nm for **78–80**, respectively, in toluene. The CPL spectra also show extraordinary FWHM of 18, 19 and 18 nm for **78–80**, respectively, in toluene. Besides, the increase of azaborine units resulted in a blue shift in the absorption and emission bands, with reported $|g_{lum}|$ values of 2.3×10^{-3} for **80**, 0.75×10^{-3} for **79**, and 1.9×10^{-3} for **78**.

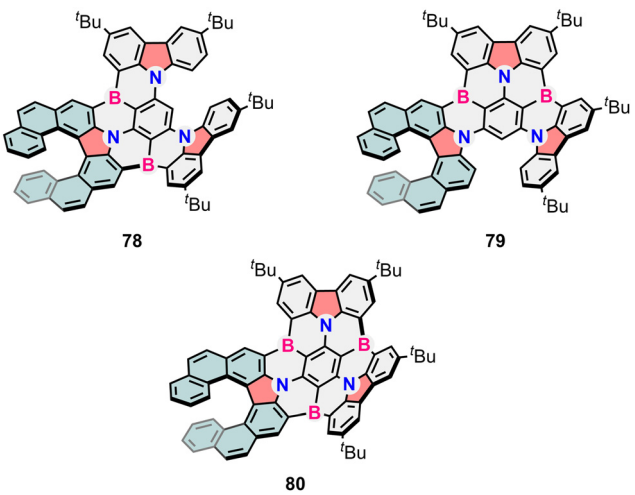

Fig. 21 Chiral nanographenes with CPL response exhibiting borazine units reported by Ravat and co-workers.

2.4.3. Oxygen-doped chiral NGs. Following with O-doped chiral NGs, a furan based double oxa[7]helicene (**81**, Fig. 22) was synthesised by Peng, Hu, and co-workers in 2020.[136] (*P*,*P*)-**81** and (*M*,*M*)-**81** exhibited CPL activity, offering a moderate g_{lum} of -0.75×10^{-3} at 506 nm for (*P*,*P*)-**81**. Compound **81** is structurally related to **6** (Section 2.1, Fig. 3) and **60** (Section 2.4.1, Fig. 16) and can help to draw a correlation between the effect of including furan rings and the CPL response. The g_{lum} value of **81** falls between those of **6** and **60**, indicating that

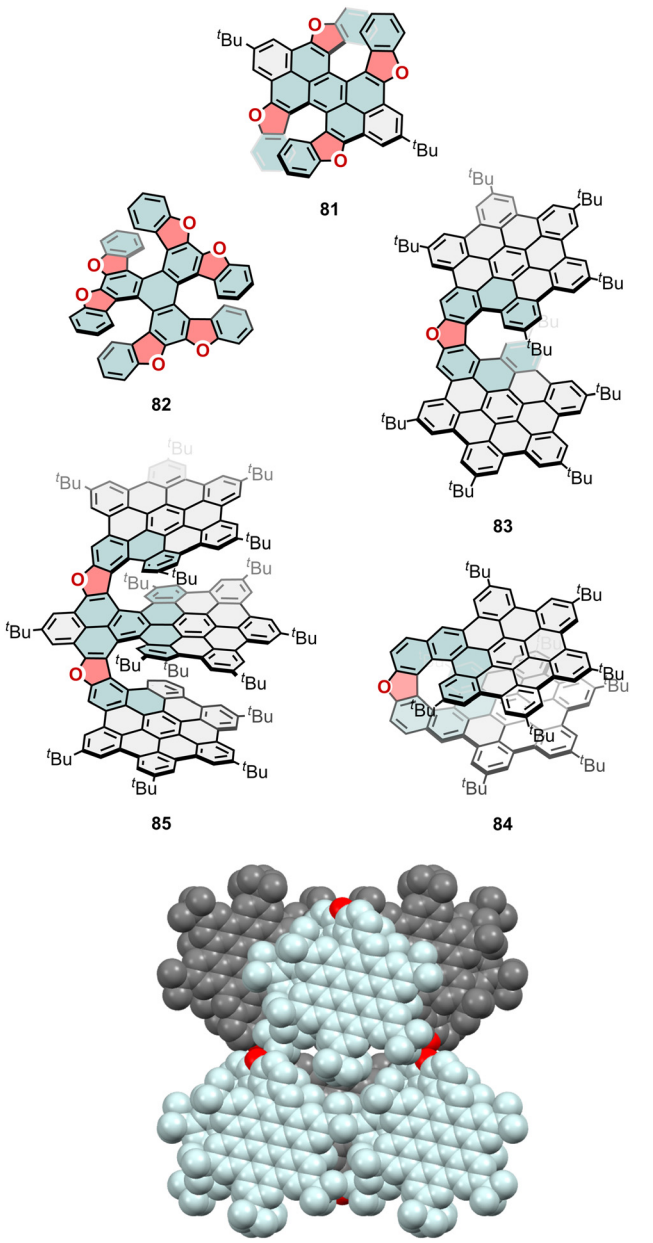

Fig. 22 Furan-containing chiral nanographenes as part of peropyrene (**81**), triphenylene (**82**), and bilayer (**83** and **84**) or trilayer (**85**) nanographenes. Crystal packing of (*M*)-**84** (bottom).

embedding furan rings into a full-carbon peropyrene-cored structure can increase the g_{lum} value. In 2021, Yang and co-workers reported the synthesis of compound **82** (Fig. 22), a triple oxa[7]helicene.[137] Compared with **81**, the triphenylene-cored **82** exhibited significantly improved g_{lum} values, reaching a g_{lum} of 1.8×10^{-3} at 492 nm for (*M*,*M*,*M*)-**82**. Compound **82** is structurally related to compound **7** (Section 2.2, Fig. 3), where both compounds exhibit a triphenylene core. The CPL response of **82** is stronger than that of **7** ($|g_{lum}| = 1.3 \times 10^{-3}$), however, the helicene size is larger for **82**. Thus, it is difficult to correlate this increase with the inclusion of furan rings or not.

Further, more extended architectures containing furan units were envisioned and reported, as it is the case of bi and trilayer structures, where furan units take relevance due to the modulation of their interlayer overlap and π-conjugation. Such is the case of a bilayer NG linked by a furan unit reported by Jux and co-workers in 2018.[138] Although in this publication the racemic resolution and chiroptical properties were not included, this was later realized in collaboration with Fuchter's group,[139] being the $|g_{lum}|$ value of **83** equal to 0.3×10^{-3} at 540 nm. This dissymmetric emission was amplified by 500 times when embedded into an achiral polydioctylfluorene (PFO) matrix ($|g_{lum}|$ of PFO:**83** blends ≈ 0.15), due to a Forster resonance energy transfer (FRET) phenomenon between the electric and magnetic dipole moments of the PFO (donor) and **83** (acceptor).

Also, by the end of 2024, Martín and co-workers reported a new example of enantioselective strategy to obtain enantiomerically pure helical bilayer NGs.[140] The prepared BINOL-based polyarene precursor was used in a monoesterification with enantiopure 1*R*-10-camphorsulfonyl chloride to afford two diastereoisomers easily isolable by flash column chromatography. Once the two enantiomers were obtained, the authors performed a Scholl oxidation to obtain the corresponding enantiomers of **84** (Fig. 22), as oxa[9]helicene-embedded bilayer NGs. Both enantiomers crystallize in the $C222_1$ space group (Fig. 22), with the molecules located in sheets parallel to the (110). Huge spaces could be found between the layers, containing high disordered solvent molecules. The chiroptical properties of **84** were studied, reaching $|g_{lum}|$ values of 2.6×10^{-3} for (*M*)-**84**. As previously observed in their full-carbon analogues (Section 2.2, Fig. 6, compounds **16** and **17**), compounds **83** and **84** evidence the effect of the overlapping of the bilayer π-system and the size of the helicene. Thus, **84** exhibits an increased CPL response compared to **83** (2.6×10^{-3} *vs.* 0.3×10^{-3}). In addition, compared with their full-carbon analogues, compounds **83** and **84** exhibit lower g_{lum} values than compounds **16** and **17**. This fact suggests that the inclusion of furane rings into bilayer NG structures is detrimental to the CPL response. In 2023, Tan and collaborators reported the CPL studies on a trilayer NG bearing two oxa[8]helicene units (**85**, Fig. 22) and compared them with its full-carbon analogue (Section 2.2, Fig. 7, compound **24**).[83] The CPL spectra of **85** showed a $|g_{lum}|$ value of 0.3×10^{-3}, which is lower than the 1×10^{-3} reported for **24**. Remarkably, the interlayer overlap is higher in **24**, which affects the photoluminescence lifetime, among other properties.

Besides furan units, O-doped heptagonal rings have been reported in literature. The synthesis of a BINOL-like atropisomeric chiral NG (**86**, Fig. 23) was described by An *et al.* in 2022.[141] The CPL of the pair of atropisomers displayed opposite signals with a $|g_{lum}|$ of 0.24×10^{-3} at 480 nm. Regarding NGs that combine O-doped and medium-sized rings, Tan and co-workers, and Miao and co-workers recently reported examples including (oxa)pentagon–heptagon (**87–91**, Fig. 23) and (oxa)pentagon–nonagon pairs, respectively.[142,143] The family reported by Tan and co-workers was composed by five members: (i) an extended HBC with two furan moieties embedded into two helicenes (**87**); (ii) its one pentagon–heptagon pair (**88**); (iii) an extended HBC with four furan moieties embedded into three helicenes (**89**); (iv) its one pentagon–heptagon derivative

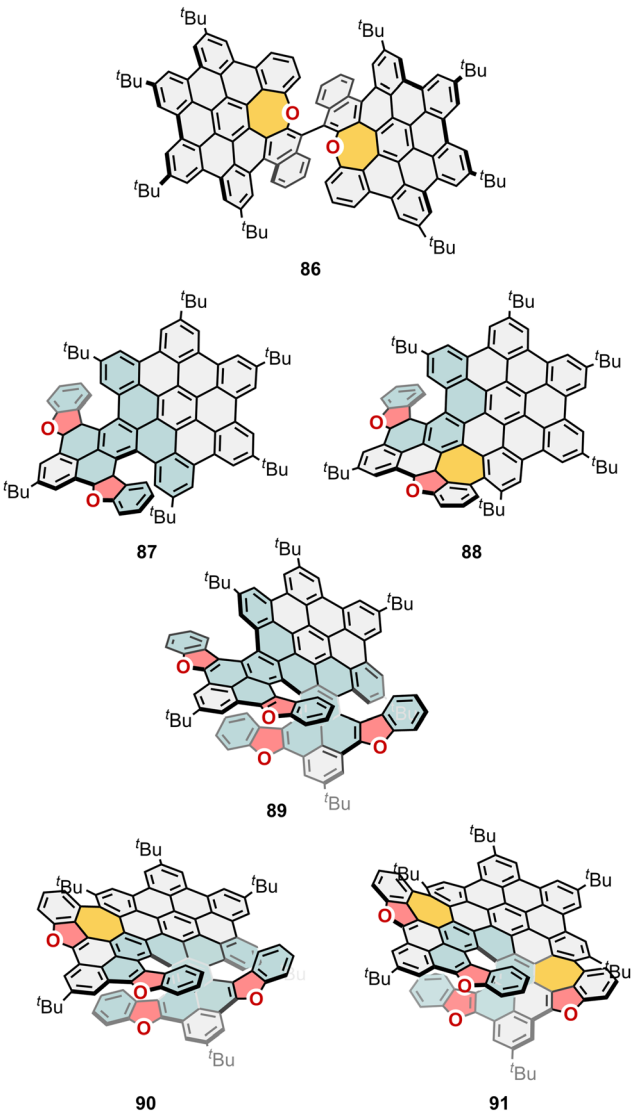

Fig. 23 Chiral nanographene embedding a BINOL as part of the π-system (**86**), and HBC-based nanographenes combining furans (**87** and **89**) and heptagon(s) (**88**, **90** and **91**).

(**90**); and (v) its two pentagon–heptagon pairs and an oxa[9]helicene derivative (**91**). The reported $|g_{lum}|$ values were evaluated as 0.6×10^{-3}, 1.5×10^{-3}, 0.5×10^{-3} 1.6×10^{-3} and 2.1×10^{-3}, respectively. Therefore, the authors conclude that increasing the pentagon–heptagon pairs in the structure will enhance the CPL response. In Miao's examples, the same trend is observed.

2.4.4. Oxygen–boron-doped chiral NGs. The introduction of boron and nitrogen atoms was an important strategy to modulate the electronics of chiral NGs. Introducing boron and oxygen atoms in CPL-active NGs is being under study, as an interesting approximation to modulate the chiroptical properties. In 2024 Babu and co-workers developed the synthesis of a BO-doped π-extended helical NG (**92**, Fig. 24).[144] Compound **92** exhibits two 5,9-dioxa-13*b*-boranaphtho[3,2,1-*de*]anthracene (DOBNA) units, fused to a central HBC moiety. The synthesis of **92** started from an acetylene-bridged DOBNA dimer from which the HBC unit was constructed through Diels–Alder and Scholl oxidation. Compound **92** exhibited multiresonance-TADF (MR-TADF) due to the presence of boron and oxygen, with lifetime values of 5 μs, and phosphorescence behaviour. The CPL spectra showed mirror image signal with negative signal for (*P*)-**92**, and positive signal for (*M*)-**92**. The $|g_{lum}|$ reached values of 2.5×10^{-3} for (*M*)-**92**.

2.4.5. Sulphur-doped chiral NGs. Other chalcogen-containing NGs exhibiting CPL have also been reported. Thus, we conclude Section 2 gathering the S- and Se-doped NGs for which the g_{lum} values have been evaluated. Two works were reported by An and co-workers, and by Xiao and co-workers. The former reported CPL studies of a sulphur- and sulphoxide-doped heptagon-containing seco-HBC (**93** and **94**, Fig. 24).[62] The $|g_{lum}|$ was determined to be 1.1×10^{-3} and 0.56×10^{-3} for **93** and **94**, respectively, at 480 nm. Due to the low Φ_F (lower than 0.01), the CPL of their Se-doped analogues was too weak to be detected. Meanwhile, due to the high ε and Φ_F, the enantiomers of **93** and **94** exhibited B_{CPL} up to 13 and 12 M^{-1} cm^{-1}, respectively. The latter reported the synthesis of a S-doped NG bearing a thiophene-containing double [6]helicene unit (**95**, Fig. 24).[145] The CPL spectra presented a maximum centred at 521 nm. Moreover, the $|g_{lum}|$ values were found to be 0.6×10^{-3} for (*P*,*P*)-**95**. Recently, Hu and co-workers reported the synthesis of different thia-helicenes-containing NGs with enhanced luminescence (**96–99**, Fig. 24).[67,146] The thia-helicene has been a class of helicene with important chiroptical features, especially ECD. However, their weak fluorescence has been an obstacle to develop CPL emitters. Isomers **96** and **97** were synthesized, exhibiting strong Φ_F of 0.83 and 0.91, respectively. In addition, the CPL responses were measured with a $|g_{lum}| = 2.2 \times 10^{-3}$ and $|g_{lum}| = 2.1 \times 10^{-3}$, respectively, performing higher values than the previously reported in 2022 peropyrene-cored thia-helicene **98** ($\Phi_F = 0.43$ and $|g_{lum}| = 1.2 \times 10^{-3}$), and its sulphone analogue **99** ($\Phi_F = 0.31$ and $|g_{lum}| = 1.1 \times 10^{-3}$). The authors attribute this CPL enhancement to the increased *m*.

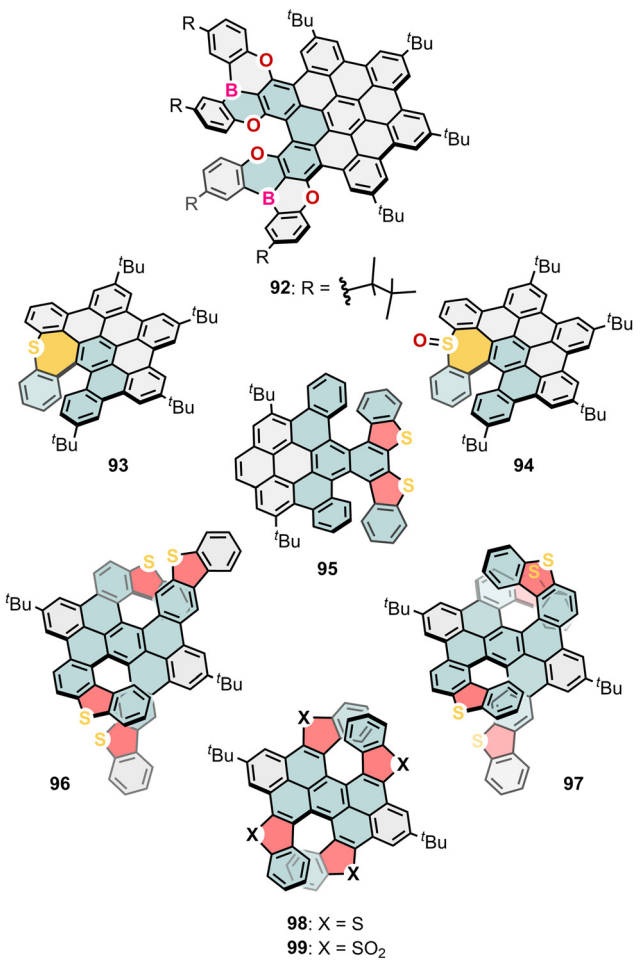

Fig. 24 DOBNA-HBC hybrid chiral nanographene (**92**), S-doped nanographenes embedding a heptagonal ring (**93** and **94**), and thiophene-containing nanographenes (**96–98**).

3. Future perspectives

3.1. Enantioselective synthesis

Achieving precise control over the chirality of NGs during synthesis is challenging and usually relies on the racemic synthesis followed by a tedious racemic resolution. Chirality induction often relies on enantioselective synthesis or post-functionalization, which can be complex, expensive, and low yielding. On the one hand, producing large quantities of chiral NGs with consistent optical properties is difficult. On the other hand, scaling up from laboratory synthesis to industrial production while maintaining purity and enantiomeric excess remains a significant hurdle.

New synthetic strategies involving enantioselective catalysis or chiral templates could offer better control over chirality while increasing yields and reducing costs.[65,98,140] Post-synthetic functionalization strategies could allow for fine-tuning of optical and electronic properties, enhancing the performance of chiral NG-based emitters.

3.2. Boosting chiroptical properties

While NG structures can be tailored for specific chiroptical properties, the vast diversity of possible structural modifications creates challenges in systematically understanding the relationships between structure, chirality, and optical behaviour. On the other hand, chiral NGs often exhibit relatively low Φ_F. This fact limits their potential in applications such as display technologies or light-emitting devices,[147] where high brightness and efficiency are crucial. Non-radiative decay channels in these molecules reduce the efficiency of light emission. Thus, finding ways to suppress such losses while maintaining chirality is still an open challenge.[148]

More critical is the fact that chiral NGs usually exhibit low g in their CPL emission, limiting the detection of the circular polarization excess. As commented before (eqn (1.5)), g_{lum} value is controlled mainly by a couple of dipole transition vectors, μ and m, which depends on non-obvious quantum mechanics.[149,150]

In the literature, some examples have been described with some success. In 2021, Narita and co-workers reported π-extended [7] and [9]helicenes (**2** and **3**, Fig. 3), revealing that the slight variation in helical length from [7] to [9] can cause an approximately 10-fold increase in the dissymmetry factors. To explain this, they studied the molecules theoretically and calculated transition dipole moments using TD-DFT. The higher $|m|$, lower $|\mu|$, and larger $\cos\theta$ of **3** than of **2** all lead to an increase in the calculated dissymmetry factor by a factor of 10 with respect to that of **2**, consistent with the trend observed experimentally.[43] Later, in 2022, following the strategy reported by Mori and co-workers for carbohelicenes,[73] Hu and co-workers also studied X-shaped double carbo[7]helicene when they exchanged terminal benzene rings with triazole, resulting in 12.8 fold increase in g_{lum} and a significant increase in Φ_F in comparison to double carbo[7]helicene.[61] Since these compounds share comparable $|\mu|$ and $\cos\theta$ values, the boost in g_{lum} can be mainly attributed to the increased $|m|$ value. Later, in 2023, Martín and co-workers reported a series of helical bilayer NGs and studied the impact of the central helicene size on μ and m. When going from [11] to [9]helicene, a simultaneous increase in $\cos\theta$ and $|m|/|\mu|$ consequently resulting in very high dissymmetry factors for [9]helicene bilayer NG in comparison to [11]helicene bilayer NG. Also related is the study presented by Feng and co-workers establishing the relationship between the geometry of HBC units linked by double [7]helicenes and their chiroptical properties.[82] Again, geometric engineering showed the role played by the relative position on the θ, μ and m values, and therefore on the final g_{lum} values.

Nevertheless, human limitations to infer the frontier molecular orbitals with precision have hampered the deep understanding on how the molecular structure influences CD and CPL performance, a future evolving field. While exploiting forbidden transitions allows for high dissymmetry factors due to an increased contribution of $|m|$ and very small $|\mu|$ this strategy often comes at the cost of lowering the absorption/emission strength, $|\mu|^2$, and consequently the photoluminescence quantum yield. An alternative approach is to engineer the molecule structure to balance the contributions of $|m|$ and $|\mu|$ and to optimize the angle between them. In a very naïve view, optimization of CPL performance at small molecule level then depends on two critical factors: (i) the molecule must be emissive, that is, dipole strength $|\mu|^2$ must be reasonably high; and (ii) the magnetic dipole transition moment $|m|$ must be also high to maintain a suitable ratio. Roughly, and considering a parallel alignment, a $|\mu|$ value of 400×10^{-20} esu cm, requires an $|m|$ value of 100×10^{-20} erg G^{-1} to achieve an impressive g_{lum} value of 1. For a figure of merit of 0.1 a $|m|$ value of 25×10^{-20} erg G^{-1} is still required. Owing to usual values for $|m|$ in single organic molecules are around 1×10^{-20} erg G^{-1}, guidelines to design molecules with such large $|m|$ values are then indispensable. Within this context our group recently managed to present a rational relationship between the magnitude of $|m|$ and the chemical structure with the aid of machine learning approaches.[151,152] In this way, it was shown that the best $|m|$ values occur for those transitions whose orbitals are fully delocalized around a helical movement. Remarkably, the magnitude of m is directly related with the surrounding area of this electron movement during the transition which, from the structure point of view, is directly related to either the number of turns or the size of the turn in helical conjugated structures.[151,153] It is also worth noting that cylindrical geometries of π-conjugated frameworks have proved to be effective strategies for increasing $|m|$ values that should be also considered when designing CPL active NGs.[154,155] Despite of these powerful structure–property correlations, in terms of chiral emission, it is the lowest-energy electronic transition $S_1 \rightarrow S_0$ the one that must be magnetically allowed without compromising the $|\mu|$. Although the introduction of substituents in selected positions with large orbital coefficients have proven to be a suitable strategy for changing orbital energy,[156] thus optimizing the symmetry and magnitude of their lowest-energy electronic transitions, further development of the corresponding general rules are still lacking. However, considering the large number of both possible substituents and substitution positions in a particular conjugated core, machine learning techniques become again the approach of choice to tackle those problems.[152] In fact, an optimization of chiroptical properties of polysubstituted [6]helicenes has demonstrated that trained neural networks are suitable tools in this field, and probably they are going to be of special focus in the near future.

3.3. Combining/hybridizing chiral NGs with other materials

Combining/hybridizing chiral NGs with other materials (*e.g.*, metal–organic frameworks, quantum dots, polymers) could also boost dissymmetry factors and enhance CPL emission. This is the case of the presence of chiral near fields in the surroundings of chiral plasmonic nanoparticles. The coupling of such dense chiral fields promotes an increased chiral light–matter interaction boosting the chiroptical responses.[157] In a

similar way, when chiral NGs are embedded in an achiral conjugated polymer matrix a remarkable phenomenon appears. In 2020, Fuchter and co-workers demonstrated a 500-fold amplification of the $|g_{lum}|$ of **82**,[158] previously reported by Jux and co-workers.[159] They rationalized that the amplification arises through electrodynamic coupling between the polymer donor's electric and magnetic transition dipoles and superhelicene acceptor, resulting in CPL resonance energy transfer. Considering the delocalized exciton in the polymer as a kind of chiral near field, an alternative mechanism may emerge which could be more broadly adopted to enhance the dissymmetry factors of NGs.[160,161] Other interesting approach is the spin-OLEDs[162–164] in which the chiral matter polarizes the electron/hole transport within the material producing a spin dependent recombination and CPL emission even in achiral emissive layers. In that case, the chiral NGs would be the media in which the so-called chiral induced spin selectivity (CISS) effect takes place.

3.4. Responsive systems

On the other hand, creating NGs that change their chiroptical properties in response to external stimuli (such as light, temperature, or pH) could lead to new classes of smart, dynamic materials for adaptive optics and sensing.[37,113,165–167] This is especially appealing as probes for the so-called CPL microscopies,[168,169] taking circular polarization as an additional information channel.

In summary, the meticulous design of the molecular structure can give optimum $|\mu|$, $|m|$ and $\cos\theta$ values, which result in high g. However, the increased contribution of $|m|$ may result in low absorption/emission strengths if $|\mu|$ is not considered, which is why smart synthetic designs are required. Hence, tunable molecular designs supported by artificial intelligence and efficient computation, can be adopted to boost dissymmetry factors in chiral NGs. Other than that, the chiroptical activity of NGs has been enhanced through aggregation and assembly in polymer matrix, although the limits of this approach have not been defined to date.

Conclusions

In this review, we have summarised recent advancements in the bottom-up synthesis of chiral NGs, including various benzenoid, non-benzenoid rings, and heteroatom-containing systems. The synthesis and study of chiral NGs have advanced at an exponential rate. In addition to the natural interest in chirality as the foundation of the phenomena of life, there is a growing interest in creating novel exotic carbon structures with various structural defects, which allows modulation of their molecular orbital structure and, thus, their photophysics. Next, Tables 1–3 summarizes the main photophysical properties reported for CPL-active NGs in this review. Despite significant efforts, finding a direct relationship between the structure of chiral NGs and their CPL emission does not seem obvious. It became clear that the random inclusion of more chiral motifs might not necessarily result in better CPL performance. Π-extension and elongation of helical motifs seem to have a more significant effect. It is still difficult to modulate the luminescence dissymmetry factor and quantum yield efficiently by adjusting the electric and magnetic transition dipole moment vectors of the $S_1 \rightarrow S_0$ transition. The balance between these two parameters is especially crucial, and to keep that in mind, designing chiral NGs remains unsolved and would require a deep rational design based on orbital engineering. The key thing here is to create delocalized HOMO/LUMO levels including the helical part of the molecule, thus ensuring that the electronic circulation takes place in the S_1 to S_0 states. This can be done placing suitable donor/acceptor groups in critical positions or incorporation electron rich motives as alkynes as part of the helical structure.[170–172] On the other hand, intense chiroptical responses can be attributed to the nature of the helical system. Higher the enclosed area of a transition, higher the strength of the corresponding signal. Combining the above-mentioned advice the designing chiral NGs would become more rational, and the actual limits could be surpassed. When looking for enhanced chiroptical response, the focus must be in a deep rational design based on orbital engineering instead of usual criteria of preparing magnificent chemical structures. In fact, very simple rationally designed structures could lead to impressive responses. Nevertheless, in any case, the generation of unprecedented complicated conjugated structures would always remain as a fascinating challenge for organic chemists. In this sense, and despite significant progress in synthesizing NGs, developing enantioselective synthetic techniques for synthesizing chiral NGs constitutes a specially challenging topic.

Moving forward, interdisciplinary approaches that combine molecular design, advanced chiral characterization, artificial intelligence (AI) methods, and computational modelling are likely to propel this field toward practical applications.[151,173] With continued research, chiral NGs could be the foundation for next-generation CPL-active materials, opening exciting possibilities in optoelectronics, bioimaging, and sensing.

Author contributions

V. K., J. L. P., S. M.-L, J. M. C., C. M. C. and A. G. C.: writing – original draft, writing – review & editing.

Data availability

Data for this article, including Chemdraw files of the reported structures, are available at Zenodo at **https://doi.org/10.5281/zenodo.14649011**.

Conflicts of interest

There are no conflicts to declare.

Appendix

Table 1 Summary of the main optical and chiroptical properties of compounds reported in Section 2.2

Compound	$\lambda_{abs,max}$ (nm)	$\varepsilon_{max}/10^3$ (M^{-1} cm^{-1})	$\lambda_{em,max}$ (nm)	Φ_F	$\lvert g_{abs}\rvert/10^{-3}$ (nm)	$\lvert g_{lum}\rvert/10^{-3}$	B_{CPL} (M^{-1} cm^{-1})	$\lvert\mu\rvert/10^{-20}$ (esu cm^{-1})	$\lvert m\rvert/10^{-20}$ (erg G^{-1})	θ (°)
1[67]	420	89.59	467	0.11	1 (423)	1	5	—	—	—
2[43]	441	11.2	495	0.250	1.24 (446)	0.77	1.1	469.2[a]	0.81[a]	84.1[a]
3[43]	452	7.1	528	0.41	10.58 (471)	7.44	12.6	407.0[a]	2.24[a]	69.6[a]
4[67]	464	—	504	0.81	6.6	0.53	—	650[b]	0.048[b]	29.8[b]
5[68]	491	—	529	0.75	0.93 (490)	0.75	—	—	—	81.7
6[61]	375	42	572	0.80	0.48 (514)	0.07	1.2	571[b]	0.097[b]	19.94[b]
7[72]	427	—	483	0.018	1.80 (427)	1.30	—	—	—	0
8[74]	592	—	612	0.58	0.69 (592)	0.78	6.8	910[a]	0.132[a]	5.78[a]
9[75]	538	85	562	0.930	7.00 (360)	0.80	32	1000[b]	0.54[b]	0[b]
10[76]	477	350	625	0.110	1.57 (550)	1.50	—	—	—	—
11[76]	479	240	625	0.082	1.88 (450)	1.50	—	—	—	—
12[77]	349	—	654	0.32	3.0 (292)	4.5	—	474.39[a]	1.99[a]	107.2[a]
13[77]	359	—	812	0.15	8.5 (492)	1.3	—	913.48[a]	2.45[a]	87.4[a]
14[77]	366	—	817	0.14	3.0 (454)	1.4	—	830.88[a]	1.76[a]	95.5[a]
15[77]	359	—	1010	0.07	1.2 (604)	—	—	916.85[a]	0.14[a]	107[a]
16[80]	518	16.8	562	0.45	8.5 (545)	7.9	168	474[a]	3.7[a]	82.47[a]
17[79]	373	136	575	0.22	36	36	81	101.6[b]	0.2627[b]	3.4[b]
18[79]	377	103.9	543	0.10	16	11	21	94.5[b]	0.1401[b]	17.78[b]
19[79]	377	125	528	0.11	10	8.9	27	83.8[b]	0.1749[b]	63.51[b]
20[80]	554	26.7	577	0.74	3.9 (560)	2.7	112	857[a]	5.5[a]	87.04[a]
21[80]	570	72	585	0.91	2.4 (580)	1.5	106	1146[a]	7.1[a]	88.23[a]
22[82]	533	—	562	0.44	18 (540)	13.2	176	748[b]	5.05[b]	80[b]
23[82]	543	—	564	0.41	10 (546)	8.7	143	735[b]	5.17[b]	82[b]
24[83]	376	—	616	0.24	4.2 (472)	1	—	—	—	—
25[65]	544	80	612	0.31	30 (559)	40	490	230[a]	2.26[a]	5.19[a]
26[65]	552	73.6	607	0.23	25 (567)	34	287	218[a]	2.25[a]	8.74[a]
27[88]	472	135	684	0.1	27.6 (640)	45	304	251[a]	3.32[a]	38.73[a]
								292[b]	3.60[b]	40.54[b]
28[90]	496	210	636	0.1	8.6 (592)	4	42	31.4[b]	0.153[b]	2.56[b]
29[91]	297	174.3	635	0.063	8 (582)	4	—	383.8[a]	2.83[a]	78.9[a]
30[92]	—	—	—	0.04	2.5 (421)	1.27	0.28	363.86[a]	1.32[a]	83.68[a]
31[93]	426	13.39	493	0.19	2.43	0.54	—	331.29[b]	0.08[b]	50.95[b]
32[93]	431	7.32	473	0.05	2.64	0.63	—	461.35[b]	0.31[b]	71.9[b]
33[93]	425	12.53	492	0.15	4.05	1.54	—	395.89[b]	0.80[b]	19.95[b]
34[97]	363	—	365	0.04	—	1.00	—	—	—	—
35[98]	361	202.214	469	—	6.3 (294)	1.9	16.7	—	—	—

[a] From $S_0 \rightarrow S_1$ transition. [b] From $S_1 \rightarrow S_0$ transition.

Table 2 Summary of the main optical and chiroptical properties of compounds reported in Section 2.3

Compound	$\lambda_{abs,max}$ (nm)	$\varepsilon_{max}/10^3$ (M^{-1} cm^{-1})	$\lambda_{em,max}$ (nm)	Φ_F	$\lvert g_{abs}\rvert/10^{-3}$ (nm)	$\lvert g_{lum}\rvert/10^{-3}$	B_{CPL} (M^{-1} cm^{-1})	$\lvert\mu\rvert/10^{-20}$ (esu cm^{-1})	$\lvert m\rvert/10^{-20}$ (erg G^{-1})	θ (°)
36[100]	398	—	508	0.22	—	0.43	—	—	—	—
37[101]	554	—	569	0.43	3.26	1	—	—	—	—
38[51]	444	66	560	0.13	2.7 (370)	0.23	—	—	—	—
39[53]	472	160	610	0.098	2.5 (580)	2	12.3	—	—	—
(*P*,*P*,*P*/*M*,*M*,*M*)-**40**[102]	517	297	643	0.28	8.2	0.3	40	—	—	—
(*P*,*P*,*M*/*M*,*M*,*P*)-**40**[102]	522	412	650	0.28	0.88	0.2	62	—	—	—
41[104]	365	145	697	0.04	3.0 (520–675)	3.0	90.5	—	—	—
42[105]	496	1.21	537	0.02	≈4.7 (307)	0.95	—	—	—	—
43[106]	509	—	542	0.47	3.5	0.94	—	—	—	—
44[107]	512	10.4	602	0.03	6.6 (553)	1.3	—	—	—	—
45[110]	356	71	480	0.13	1.3	0.4	—	—	—	—
46[110]	342	53	554	0.08	1.5 (294)	0.7	1.30	—	—	—
47[111]	355	80	456	0.11	3.9 (281)	—	—	113[a]	0.0360[a]	118.69[a]

[a] From $S_0 \rightarrow S_1$ transition.

Table 3 Summary of the main optical and chiroptical properties of compounds reported in Section 2.4

Compound	$\lambda_{abs,max}$ (nm)	$\varepsilon_{max}/10^3$ (M^{-1} cm^{-1})	$\lambda_{em,max}$ (nm)	Φ_F	$\lvert g_{abs}\rvert/10^{-3}$ (nm)	$\lvert g_{lum}\rvert/10^{-3}$	B_{CPL} (M^{-1} cm^{-1})	$\lvert\mu\rvert/10^{-20}$ (esu cm^{-1})	$\lvert m\rvert/10^{-20}$ (erg G^{-1})	θ (°)
48[113]	351	85	457	0.04	0.65 (352)	0.8	1.40	—	—	—
49[106]	513	—	552	0.12	1.9	16	—	—	—	—
50[106]	510	—	536	0.48	2	9.1	—	—	—	—
51[106]	547	—	609	0.56	2.4	6	—	—	—	—
52[106]	510	—	539	0.52	3	6	—	—	—	—
53[106]	510	—	543	0.51	2.1	2.4	—	—	—	—
54[114]	350	—	450	—	—	≈0.23	—	—	—	—
55[115]	331	109.65	517	—	3.1 (432)	2	—	—	—	—
56[116]	452	11	503	0.33	6.7	2.4	9.1	—	—	—
57[116]	580	16	588	0.32	10	7.0	95.2	—	—	—
58[117]	382	108.4	542	0.75	3.91	1.12	45.77	245.73[b]	0.362[b]	166.56[b]
59[118]	360	113	595	0.40	2.98 (469)	1.30	28.57	327[b]	0.186[b]	178.87[b]
60[120]	368	69	553	0.96	1.3 (511)	0.91	30.1	57[b]	0.097[b]	20[b]
61[121]	420	3.52	531	0.45	44.6	2.2	173	548.02[a]	0.707[a]	158.83[a]
62[122]	—	88.0	646	0.44	1.2	0.73	14.13	345.49[b]	0.40[b]	87.29[b]
63[122]	—	81.4	582	0.43	1.4	0.89	15.57	150.42[b]	0.06[b]	60.94[b]
64[122]	—	67.2	576	0.79	2.9	5.5	145.9	237.77[b]	0.82[b]	52.12[b]
65[129]	489	19.5	528	0.80	—	0.75	—	—	—	—
66[130]	490	20	526	0.64	1.9 (496)	1.1	—	—	—	—
67[131]	504	36	522	0.65	2.5 (492)	0.90	14.6	—	—	—
68[131]	524	—	567	0.99	8.5 (368)	1	—	—	—	—
69[131]	518	—	541	0.90	6.3 (368)	1	—	—	—	—
70[132]	545	—	585	0.66	8.6	2.5	45.8	689.3[b]	0.80[b]	24.4[b]
71[132]	548	—	595	0.68	7.4	2.7	41.5	755.9[b]	0.30[b]	136.8[b]
72[132]	553	—	598	0.64	3.1	2.7	58.7	682.5[b]	1.5[b]	48.7[b]
73[132]	622	—	675	0.11	4.7	2.9	2.0	464.6[b]	4.6[b]	80.0[b]
74[132]	595	—	641	0.01	6.6	5.0	4.0	352.2[b]	4.3[b]	79.2[b]
75[133]	627	—	660	1.00	3.3 (502)	2.00	28.5	552[a]	0.46[a]	0[a]
76[133]	650	—	684	0.99	3.1 (518)	2.00	37.1	617[a]	0.41[a]	0[a]
77[133]	662	—	696	0.90	2.6 (526)	2.00	40.0	736[a]	0.41[a]	0[a]
78[135]	495	56	498	0.83	2.7	1.9	—	376.1[b]	1.23[b]	84.26[b]
79[135]	493	57	500	0.85	1.0	0.75	—	691.3[b]	1.45[b]	83.68[b]
80[135]	479	24	485	0.59	4.1	2.3	—	229.4[b]	1.85[b]	81.95[b]
81[136]	375	—	511	0.71	—	0.75	—	—	—	—
82[137]	262	—	492	0.04	≈5.95 (314)	≈1.7	—	0.63[b]	0.00053[b]	45[b]
83[139]	525	—	620	0.85	2.00 (509)	0.30	—	—	—	—
84[140]	371	146.9	500	0.30	2.7 (452)	2.6	—	—	—	—
85[83]	364	—	565	0.37	2.7 (378)	0.3	—	—	—	—
86[141]	360	170	475	0.02	—	0.24	—	—	—	—
87[142]	503	—	535	0.49	5.2	0.6	10–8	—	—	—
88[142]	542	—	622	0.03	3.3	1.5	1.7	—	—	—
89[142]	575	—	611	0.54	4.6	0.5	13.9	—	—	—
90[142]	590	—	639	0.26	4.0	1.6	14.7	—	—	—
91[142]	594	—	644	0.10	3.6	2.1	7.1	—	—	—
92[144]	400	—	546	0.50	—	≈2.4	≈31	412[b]	0.34[b]	175.34[b]
93[62]	351	130	475	0.18	—	1.1	13	—	—	—
94[62]	353	140	473	0.30	—	0.56	12	—	—	—
95[145]	387	61	517	0.03	≈14.5 (352)	≈0.55	—	—	—	—
96[67]	392	930	569	0.83	4 (310)	2.2	84.9	499[b]	0.456[b]	2.4[b]
97[67]	397	680	583	0.91	5.3 (365)	2.1	65	435[b]	0.632[b]	54[b]
98[146]	387	—	558	0.43	14 (327)	1.2	—	782.69[b]	0.254[b]	12.04[b]
99[146]	420	—	614	0.31	7.2 (323)	1.1	—	824.73[b]	0.275[b]	21.87[b]

[a] From $S_0 \rightarrow S_1$ transition. [b] From $S_1 \rightarrow S_0$ transition.

Acknowledgements

This work has received funding from: Grant PID2021-127521NB-I00 and grant PID2022-137403NA-I00 funded by MICIU/AEI/10.13039/501100011033 and by ERDF/EU. C. M. C. acknowledges grant RYC2023-044652-I funded by MICIU/AEI/10.13039/501100011033 and by ESF+. J. L. P. acknowledges Grant PRE2022-102320 funded by MICIU/AEI/10.13039/501100011033 and by ESF+.

Notes and references

1 J. X. Flores-Lasluisa, M. Navlani-García, Á. Berenguer-Murcia, E. Morallón and D. Cazorla-Amorós, *Front. Mater.*, 2024, **11**, 1381363.
2 D. R. Lobato-Peralta, P. U. Okoye and C. Alegre, *J. Power Sources*, 2024, **617**, 235140.
3 Q. Zheng, Z. Hu, L. Liu, H. Lu, X. Wang, Y. Lei, C. Han and W. Li, *J. Mater. Chem. A*, 2024, **12**, 21531–21552.

4 V. Meunier, G. Bepete, M.-S. Cao, Y. Chen, C. de Tomas, J. Di, C. Ewels, N. Koratkar, Q. Li, C. Liu, N. Sheremetyeva and M. Terrones, *Carbon*, 2024, **229**, 119488.
5 V. Georgakilas, J. A. Perman, J. Tucek and R. Zboril, *Chem. Rev.*, 2015, **115**, 4744–4822.
6 P. R. Wallace, *Phys. Rev.*, 1947, **71**, 622–634.
7 K. S. Novoselov, A. K. Geim, S. V. Morozov, D. Jiang, Y. Zhang, S. V. Dubonos, I. V. Grigorieva and A. A. Firsov, *Science*, 2004, **306**, 666–669.
8 A. K. Geim and K. S. Novoselov, *Nat. Mater.*, 2007, **6**, 183–191.
9 E. L. Wolf, *Applications of Graphene: An Overview*, Springer, New York, 2014.
10 L. Chen, Y. Hernandez, X. Feng and K. Müllen, *Angew. Chem., Int. Ed.*, 2012, **51**, 7640–7654.
11 P. Izquierdo-García, J. M. Fernández-García and N. Martín, *J. Am. Chem. Soc.*, 2024, **146**, 32222–32234.
12 R. R. Nair, P. Blake, A. N. Grigorenko, K. S. Novoselov, T. J. Booth, T. Stauber, N. M. R. Peres and A. K. Geim, *Science*, 2008, **320**, 1308.
13 G. M. Paternò, Goudappagouda, Q. Chen, G. Lanzani, F. Scotognella and A. Narita, *Adv. Opt. Mater.*, 2021, **9**, 2100508.
14 Y. Gu, Z. Qiu and K. Müllen, *J. Am. Chem. Soc.*, 2022, **144**, 11499–11524.
15 L. Chen, Y. Hernandez, X. Feng and K. Müllen, *Angew. Chem., Int. Ed.*, 2012, **51**, 7640–7654.
16 R. Sekiya and T. Haino, *Chem. – Eur. J.*, 2021, **27**, 187–199.
17 E. Clar and C. T. Ironside, *Proc. Chem. Soc.*, 1958, 125–156.
18 E. Clar, C. T. Ironside and M. Zander, *J. Chem. Soc.*, 1959, 142–147.
19 A. Halleux, R. H. Martin and G. S. D. King, *Helv. Chim. Acta*, 1958, **41**, 1177–1183.
20 Y. Segawa, H. Ito and K. Itami, *Nat. Rev. Mater.*, 2016, **1**, 1–14.
21 A. Narita, X. Y. Wang, X. Feng and K. Müllen, *Chem. Soc. Rev.*, 2015, **44**, 6616–6643.
22 A. V. Gulevskaya and D. I. Tonkoglazova, *Adv. Synth. Catal.*, 2022, **364**, 2502–2539.
23 K. M. Magiera, V. Aryal and W. A. Chalifoux, *Org. Biomol. Chem.*, 2020, **18**, 2372–2386.
24 M. Ball, Y. Zhong, Y. Wu, C. Schenck, F. Ng, M. Steigerwald, S. Xiao and C. Nuckolls, *Acc. Chem. Res.*, 2015, **48**, 267–276.
25 Y. Zhang, S. H. Pun and Q. Miao, *Chem. Rev.*, 2022, **122**, 14554–14593.
26 R. Sekiya, S. Arimura, H. Moriguchi and T. Haino, *Nanoscale*, 2025, **17**, 774–787.
27 S. Míguez-Lago, J. P. Mora-Fuentes, C. M. Cruz and A. G. Campaña, in *Helicenes: Synthesis, Properties and Applications*, ed. J. Crassous, I. G. Stará and I. Starý, Wiley-VCH, Weinheim, 2022, vol. 9, pp. 283–328.
28 H. V. Anderson, N. D. Gois and W. A. Chalifoux, *Org. Chem. Front.*, 2023, **10**, 4167–4197.
29 L. Qin, J. Xie, B. Wu, H. Hong, S. Yang, Z. Ma, C. Li, G. Zhang, X. S. Zhang, K. Liu and D. Zhang, *J. Am. Chem. Soc.*, 2024, **146**, 12206–12214.
30 P. Izquierdo-García, J. M. Fernández-García, I. Fernández, J. Perles and N. Martín, *J. Am. Chem. Soc.*, 2021, **143**, 11864–11870.
31 P. Izquierdo-García, J. M. Fernández-García, J. Perles, I. Fernández and N. Martín, *Angew. Chem., Int. Ed.*, 2023, **62**, e202215655.
32 S. Li, R. Li, Y. K. Zhang, S. Wang, B. Ma, B. Zhang and P. An, *Chem. Sci.*, 2023, **14**, 3286–3292.
33 Y. Deng, M. Wang, Y. Zhuang, S. Liu, W. Huang and Q. Zhao, *Light: Sci. Appl.*, 2021, **10**, 76.
34 Y. Xuefeng, G. Xiaoqing, Z. You-Xuan, K. Hua, C. Chuan-Feng, L. Minghua, D. Pengfei and T. Zhiyong, *CCS Chem.*, 2023, **5**, 2760–2789.
35 M. Saqlain, H. M. Zohaib, S. Qamar, H. Malik and H. Li, *Coord. Chem. Rev.*, 2024, **501**, 215559.
36 J. Liu, Z.-P. Song, L.-Y. Sun, B.-X. Li, Y.-Q. Lu and Q. Li, *Responsive Mater.*, 2023, **1**, e20230005.
37 K. Takaishi, C. Maeda and T. Ema, *Chirality*, 2023, **35**, 92–103.
38 G. A. Hembury, V. V. Borovkov and Y. Inoue, *Chem. Rev.*, 2008, **108**, 1–73.
39 Y. Zhong, Z. Wu, Y. Zhang, B. Dong and X. Bai, *InfoMat*, 2023, **5**, e12392.
40 O. G. Willis, F. Zinna and L. Di Bari, *Angew. Chem., Int. Ed.*, 2023, **62**, e202302358.
41 Y. Nagata and T. Mori, *Front. Chem.*, 2020, **8**, 448.
42 L. Arrico, L. Di Bari and F. Zinna, *Chem. – Eur. J.*, 2021, **27**, 2920–2934.
43 Z. Qiu, C. W. Ju, L. Frédéric, Y. Hu, D. Schollmeyer, G. Pieters, K. Müllen and A. Narita, *J. Am. Chem. Soc.*, 2021, **143**, 4661–4667.
44 R. Li, D. Wang, S. Li and P. An, *Beilstein J. Org. Chem.*, 2023, **19**, 736–751.
45 H. Luo and J. Liu, *Angew. Chem., Int. Ed.*, 2024, **63**, e202410759.
46 Y. Zhu and J. Wang, *Acc. Chem. Res.*, 2023, **56**, 363–373.
47 Y. Liu, X. Gao, B. Zhao and J. Deng, *Nanoscale*, 2024, **16**, 6853–6875.
48 X. Yan, H. Zhao, K. Zhang, Z. Zhang, Y. Chen and L. Feng, *ChemPlusChem*, 2023, **88**, e202200428.
49 N. Suzuki, Y. Wang, P. Elvati, Z.-B. Qu, K. Kim, S. Jiang, E. Baumeister, J. Lee, B. Yeom, J. H. Bahng, J. Lee, A. Violi and N. A. Kotov, *ACS Nano*, 2016, **10**, 1744–1755.
50 H. V. Anderson, N. D. Gois and W. A. Chalifoux, *Org. Chem. Front.*, 2023, **10**, 4167–4197.
51 C. M. Cruz, I. R. Márquez, I. F. A. Mariz, V. Blanco, C. Sánchez-Sánchez, J. M. Sobrado, J. A. Martín-Gago, J. M. Cuerva, E. Maçôas and A. G. Campaña, *Chem. Sci.*, 2018, **9**, 3917–3924.
52 I. R. Márquez, S. Castro-Fernández, A. Millán and A. G. Campaña, *Chem. Commun.*, 2018, **54**, 6705–6718.
53 C. M. Cruz, S. Castro-Fernández, E. Maçôas, J. M. Cuerva and A. G. Campaña, *Angew. Chem., Int. Ed.*, 2018, **57**, 14782–14786.
54 Y. Zhang, S. H. Pun and Q. Miao, *Chem. Rev.*, 2022, **122**, 14554–14593.

55 M. Stępień, E. Gońka, M. Żyła and N. Sprutta, *Chem. Rev.*, 2017, **117**, 3479–3716.
56 A. Borissov, Y. K. Maurya, L. Moshniaha, W. S. Wong, M. Żyła-Karwowska and M. Stępień, *Chem. Rev.*, 2022, **122**, 565–788.
57 M. M. Martin, F. Hampel and N. Jux, *Chem. – Eur. J.*, 2020, **26**, 10210–10212.
58 Y. Shen and C. F. Chen, *Chem. Rev.*, 2012, **112**, 1463–1535.
59 H. Luo and J. Liu, *Angew. Chem., Int. Ed.*, 2024, **63**, e202410759.
60 Chaolumen, I. A. Stepek, K. E. Yamada, H. Ito and K. Itami, *Angew. Chem., Int. Ed.*, 2021, **60**, 23508–23532.
61 J. Hong, X. Xiao, H. Liu, E. Dmitrieva, A. A. Popov, Z. Yu, M.-D. Li, T. Ohto, J. Liu, A. Narita, P. Liu, H. Tada, X.-Y. Cao, X.-Y. Wang, Y. Zou, K. Müllen and Y. Hu, *Chem. – Eur. J.*, 2022, **28**, e202202243.
62 R. Li, B. Ma, S. Li, C. Lu and P. An, *Chem. Sci.*, 2023, **14**, 8905–8913.
63 V. Kumar, S. D. Dongre, G. Venugopal, A. Narayanan and S. S. Babu, *Chem. Commun.*, 2024, **60**, 11944–11947.
64 M. M. Martin, F. Hampel and N. Jux, *Chem. – Eur. J.*, 2020, **26**, 10210–10212.
65 F. Morita, Y. Kishida, Y. Sato, H. Sugiyama, M. Abekura, J. Nogami, N. Toriumi, Y. Nagashima, T. Kinoshita, G. Fukuhara, M. Uchiyama, H. Uekusa and K. Tanaka, *Nat. Synth.*, 2024, **3**, 774–786.
66 J. B. Birks, D. J. S. Birch, E. Cordemans and E. Vander Donckt, *Chem. Phys. Lett.*, 1976, **43**, 33–36.
67 Y. Ma, L. Zhou, J. Tan, W. Sun, Y. Zou and Y. Hu, *Adv. Opt. Mater.*, 2025, **13**, 2402446.
68 R. Yamano, Y. Shibata and K. Tanaka, *Chem. – Eur. J.*, 2018, **24**, 6364–6370.
69 W. Yang, G. Longhi, S. Abbate, A. Lucotti, M. Tommasini, C. Villani, V. J. Catalano, A. O. Lykhin, S. A. Varganov and W. A. Chalifoux, *J. Am. Chem. Soc.*, 2017, **139**, 13102–13109.
70 A. Bernhardt, D. Čavlović, M. Mayländer, O. Blacque, C. M. Cruz, S. Richert and M. Juríček, *Angew. Chem., Int. Ed.*, 2024, **63**, e202318254.
71 Y. Hu, X.-Y. Wang, P.-X. Peng, X.-C. Wang, X.-Y. Cao, X. Feng, K. Müllen and A. Narita, *Angew. Chem., Int. Ed.*, 2017, **56**, 3374–3378.
72 H. Tanaka, Y. Kato, M. Fujiki, Y. Inoue and T. Mori, *J. Phys. Chem. A*, 2018, **122**, 7378–7384.
73 H. Tanaka, M. Ikenosako, Y. Kato, M. Fujiki, Y. Inoue and T. Mori, *Commun. Chem.*, 2018, **1**, 38.
74 Y. Dong, Z. Zhang, Y. Hashikawa, H. Meng, F. Bai, K. Itami and Chaolumen, *Angew. Chem., Int. Ed.*, 2024, **63**, e202406927.
75 J. K. Li, X. Y. Chen, W. L. Zhao, Y. L. Guo, Y. Zhang, X. C. Wang, A. C. H. Sue, X. Y. Cao, M. Li, C. F. Chen and X. Y. Wang, *Angew. Chem., Int. Ed.*, 2023, **62**, e202215367.
76 J. Wang, C. Shen, G. Zhang, F. Gan, Y. Ding and H. Qiu, *Angew. Chem., Int. Ed.*, 2022, **61**, e202115979.
77 G. Huo, W. Xu, J. Hu, Y. Han, W. Fan, W. Wang, Z. Sun, H. Yang and J. Wu, *Angew. Chem., Int. Ed.*, 2025, **64**, e202416707.
78 P. J. Evans, J. Ouyang, L. Favereau, J. Crassous, I. Fernández, J. Perles and N. Martín, *Angew. Chem., Int. Ed.*, 2018, **57**, 6774–6779.
79 P. Izquierdo-García, J. M. Fernández-García, S. Medina Rivero, M. Šámal, J. Rybáček, L. Bednárová, S. Ramírez-Barroso, F. J. Ramírez, R. Rodríguez, J. Perles, D. García-Fresnadillo, J. Crassous, J. Casado, I. G. Stará and N. Martín, *J. Am. Chem. Soc.*, 2023, **145**, 11599–11610.
80 W. Niu, Y. Fu, Z.-L. Qiu, C. J. Schürmann, S. Obermann, F. Liu, A. A. Popov, H. Komber, J. Ma and X. Feng, *J. Am. Chem. Soc.*, 2023, **145**, 26824–26832.
81 K. Uehara, H. Kano, K. Matsuo, H. Hayashi, M. Fujiki, H. Yamada and N. Aratani, *ChemPhotoChem*, 2021, **5**, 974–978.
82 W. Niu, Y. Fu, Q. Deng, Z. L. Qiu, F. Liu, A. A. Popov, H. Komber, J. Ma and X. Feng, *Angew. Chem., Int. Ed.*, 2024, **63**, e202319874.
83 Y. Y. Ju, L. Chai, K. Li, J. F. Xing, X. H. Ma, Z. L. Qiu, X. J. Zhao, J. Zhu and Y. Z. Tan, *J. Am. Chem. Soc.*, 2023, **145**, 2815–2821.
84 W. Cui, Z. Jin, W. Fu and C. Shen, *Chin. Chem. Lett.*, 2024, **35**, 109667.
85 S. Ma, J. Gu, C. Lin, Z. Luo, Y. Zhu and J. Wang, *J. Am. Chem. Soc.*, 2020, **142**, 16887–16893.
86 Y. Zhu, X. Guo, Y. Li and J. Wang, *J. Am. Chem. Soc.*, 2019, **141**, 5511–5517.
87 Y. Chen, C. Lin, Z. Luo, Z. Yin, H. Shi, Y. Zhu and J. Wang, *Angew. Chem., Int. Ed.*, 2021, **60**, 7796–7801.
88 Y.-J. Shen, N.-T. Yao, L.-N. Diao, Y. Yang, X.-L. Chen and H.-Y. Gong, *Angew. Chem., Int. Ed.*, 2023, **62**, e202300840.
89 K. Zhu, Z. Li, J. Liang, K. Zou, Y. Shen and H. Gong, *Angew. Chem., Int. Ed.*, 2024, **63**, e202409713.
90 Y.-J. Shen, L.-J. Peng, L.-N. Diao, N.-T. Yao, W.-K. Chen, Y. Yang, M. Qiu, W.-X. Zhu, X. Li, X.-Y. Wang and H.-Y. Gong, *Org. Lett.*, 2024, **26**, 7279–7284.
91 J. Tan, X. Xu, J. Liu, S. Vasylevskyi, Z. Lin, R. Kabe, Y. Zou, K. Müllen, A. Narita and Y. Hu, *Angew. Chem., Int. Ed.*, 2023, **62**, e202218494.
92 A. K. Swain, K. Radacki, H. Braunschweig and P. Ravat, *J. Org. Chem.*, 2022, **87**, 993–1000.
93 A. Swain, K. Radacki, H. Braunschweig and P. Ravat, *Chem. Sci.*, 2024, **15**, 11737–11747.
94 B. P. Benke, L. Hertwig, X. Yang, F. Rominger and M. Mastalerz, *Eur. J. Org. Chem.*, 2021, 72–76.
95 P.-C. Zhu, Y. Liu, L.-H. Peng and C. Zhang, *Tetrahedron Lett.*, 2014, **55**, 521–524.
96 C. Tang, H. Han, R. Zhang, L. S. de Moraes, Y. Qi, G. Wu, C. G. Jones, I. H. Rodriguez, Y. Jiao, W. Liu, X. Li, H. Chen, L. Bancroft, X. Zhao, C. L. Stern, Q.-H. Guo, M. D. Krzyaniak, M. R. Wasielewski, H. M. Nelson, P. Li and J. F. Stoddart, *J. Am. Chem. Soc.*, 2024, **146**, 20158–20167.
97 Y. Wada, K. Shinohara and T. Ikai, *Chem. Commun.*, 2019, **55**, 11386–11389.
98 M. Buendía, J. M. Fernández-García, J. Perles, S. Filippone and N. Martín, *Nat. Synth.*, 2024, **3**, 545–553.

99 Y. Zhou, X. Zhang, B. Yuan, D. Lu, G.-L. Zhuang and P. Du, *Org. Lett.*, 2024, **26**, 5635–5639.
100 Q. Xu, C. Wang, J. He, X. Li, Y. Wang, X. Chen, D. Sun and H. Jiang, *Org. Chem. Front.*, 2021, **8**, 2970–2976.
101 J. Bergner, J. Borstelmann, L. M. Cavinato, J. P. Fuenzalida-Werner, C. Walla, H. Hinrichs, P. Schulze, F. Rominger, R. D. Costa, A. Dreuw and M. Kivala, *Chem. – Eur. J.*, 2024, **30**, e202303336.
102 C. M. Cruz, I. R. Márquez, S. Castro-Fernández, J. M. Cuerva, E. Maçôas and A. G. Campaña, *Angew. Chem., Int. Ed.*, 2019, **58**, 8068–8072.
103 S. Castro-Fernández, C. M. Cruz, I. F. A. Mariz, I. R. Márquez, V. G. Jiménez, L. Palomino-Ruiz, J. M. Cuerva, E. Maçôas and A. G. Campaña, *Angew. Chem., Int. Ed.*, 2020, **59**, 7139–7145.
104 S. Míguez-Lago, I. F. A. Mariz, M. A. Medel, J. M. Cuerva, E. Maçôas, C. M. Cruz and A. G. Campaña, *Chem. Sci.*, 2022, **13**, 10267–10272.
105 Z. Qi, H. Shang, B. Ji, Y. Shi, T. Ye, Y. Li and J. Xiao, *J. Org. Chem.*, 2023, **88**, 14550–14558.
106 J. Borstelmann, L. Schneider, F. Rominger, F. Deschler and M. Kivala, *Angew. Chem., Int. Ed.*, 2024, **63**, e202405570.
107 L. Yang, Y. Y. Ju, M. A. Medel, Y. Fu, H. Komber, E. Dmitrieva, J. J. Zhang, S. Obermann, A. G. Campaña, J. Ma and X. Feng, *Angew. Chem., Int. Ed.*, 2023, **62**, e202216193.
108 G. González Miera, S. Matsubara, H. Kono, K. Murakami and K. Itami, *Chem. Sci.*, 2022, **13**, 1848–1868.
109 J. Urieta-Mora, M. Krug, W. Alex, J. Perles, I. Fernández, A. Molina-Ontoria, D. M. Guldi and N. Martín, *J. Am. Chem. Soc.*, 2020, **142**, 4162–4172.
110 M. A. Medel, R. Tapia, V. Blanco, D. Miguel, S. P. Morcillo and A. G. Campaña, *Angew. Chem., Int. Ed.*, 2021, **60**, 6094–6100.
111 M. A. Medel, C. M. Cruz, D. Miguel, V. Blanco, S. P. Morcillo and A. G. Campaña, *Angew. Chem., Int. Ed.*, 2021, **60**, 22051–22056.
112 P. An, R. Li, B. Ma, R.-Y. He, Y.-K. Zhang, M.-J. Xiao and B. Zhang, *Angew. Chem., Int. Ed.*, 2021, **60**, 24478–24483.
113 M. A. Medel, L. Hortigüela, V. Lloveras, J. Catalán-Toledo, D. Miguel, A. J. Mota, N. Crivillers, A. G. Campaña and S. P. Morcillo, *ChemistryEurope*, 2023, **1**, e202300021.
114 F. Gan, C. Shen, W. Cui and H. Qiu, *J. Am. Chem. Soc.*, 2023, **145**, 5952–5959.
115 F. Gan, G. Zhang, J. Liang, C. Shen and H. Qiu, *Angew. Chem., Int. Ed.*, 2024, **63**, e202320076.
116 S. Qiu, A. C. Valdivia, W. Zhuang, F. F. Hung, C. M. Che, J. Casado and J. Liu, *J. Am. Chem. Soc.*, 2024, **146**, 16161–16172.
117 V. Kumar, G. Venugopal, A. B. Jadhav, S. D. Dongre, R. Gonnade, J. Kumar, P. C. Ruer, B. Hupp, A. Steffen and S. S. Babu, *Angew. Chem., Int. Ed.*, 2025, **64**, e202422125.
118 X. Wang, J. Bai, Y. Shen, Z. Li and H. Gong, *Angew. Chem., Int. Ed.*, 2025, **64**, e202417745.
119 D. Reger, P. Haines, K. Y. Amsharov, J. A. Schmidt, T. Ullrich, S. Bönisch, F. Hampel, A. Görling, J. Nelson, K. E. Jelfs, D. M. Guldi and N. Jux, *Angew. Chem., Int. Ed.*, 2021, **60**, 18073–18081.
120 J. Hong, X. Xiao, H. Liu, E. Dmitrieva, A. A. Popov, Z. Yu, M. Li, T. Ohto, J. Liu, A. Narita, P. Liu, H. Tada, X. Cao, X. Wang, Y. Zou, K. Müllen and Y. Hu, *Chem. – Eur. J.*, 2022, **28**, e202202243.
121 J. Liu, J. Hong, Z. Liao, J. Tan, H. Liu, E. Dmitrieva, L. Zhou, J. Ren, X. Y. Cao, A. A. Popov, Y. Zou, A. Narita and Y. Hu, *Angew. Chem., Int. Ed.*, 2024, **63**, e202400172.
122 S. D. Dongre, G. Venugopal, V. Kumar, A. B. Jadhav, J. Kumar and S. S. Babu, *Angew. Chem., Int. Ed.*, 2024, e202420767.
123 T. Ikeda, T. Masuda, T. Hirao, J. Yuasa, H. Tsumatori, T. Kawai and T. Haino, *Chem. Commun.*, 2012, **48**, 6025.
124 J. Kumar, T. Nakashima, H. Tsumatori, M. Mori, M. Naito and T. Kawai, *Chem. – Eur. J.*, 2013, **19**, 14090–14097.
125 B. Liu, M. Böckmann, W. Jiang, N. L. Doltsinis and Z. Wang, *J. Am. Chem. Soc.*, 2020, **142**, 7092–7099.
126 X. Tian, K. Shoyama, B. Mahlmeister, F. Brust, M. Stolte and F. Würthner, *J. Am. Chem. Soc.*, 2023, **145**, 9886–9894.
127 S. E. Penty, G. R. F. Orton, D. J. Black, R. Pal, M. A. Zwijnenburg and T. A. Barendt, *J. Am. Chem. Soc.*, 2024, **146**, 5470–5479.
128 Y. Yu, C. Wang, F.-F. Hung, C. Chen, D. Pan, C.-M. Che and J. Liu, *J. Am. Chem. Soc.*, 2024, **146**, 22600–22611.
129 Z. Sun, C. Yi, Q. Liang, C. Bingi, W. Zhu, P. Qiang, D. Wu and F. Zhang, *Org. Lett.*, 2020, **22**, 209–213.
130 Z. Sun, C. Yu, N. Zhang, L. Li, Y. Jiao, P. Thiruvengadam, D. Wu and F. Zhang, *Org. Lett.*, 2022, **24**, 6670–6675.
131 D. Tan, J. Dong, T. Ma, Q. Feng, S. Wang and D. Yang, *Angew. Chem., Int. Ed.*, 2023, **62**, e202304711.
132 Y.-Y. Ju, L.-E. Xie, J.-F. Xing, Q.-S. Deng, X.-W. Chen, L.-X. Huang, G.-H. Nie, Y.-Z. Tan and B. Zhang, *Angew. Chem., Int. Ed.*, 2025, **64**, e202414383.
133 J.-K. Li, X.-Y. Chen, Y.-L. Guo, X.-C. Wang, A. C.-H. Sue, X.-Y. Cao and X.-Y. Wang, *J. Am. Chem. Soc.*, 2021, **143**, 17958–17963.
134 F. Zhang, F. Rauch, A. Swain, T. B. Marder and P. Ravat, *Angew. Chem., Int. Ed.*, 2023, **62**, e202218965.
135 F. Zhang, V. Brancaccio, F. Saal, U. Deori, K. Radacki, H. Braunschweig, P. Rajamalli and P. Ravat, *J. Am. Chem. Soc.*, 2024, **146**, 29782–29791.
136 H. Chang, H. Liu, E. Dmitrieva, Q. Chen, J. Ma, P. He, P. Liu, A. A. Popov, X.-Y. Cao, X.-Y. Wang, Y. Zou, A. Narita, K. Müllen, H. Peng and Y. Hu, *Chem. Commun.*, 2020, **56**, 15181–15184.
137 F. Zhou, Z. Huang, Z. Huang, R. Cheng, Y. Yang and J. You, *Org. Lett.*, 2021, **23**, 4559–4563.
138 D. Reger, P. Haines, F. W. Heinemann, D. M. Guldi and N. Jux, *Angew. Chem., Int. Ed.*, 2018, **57**, 5938–5942.
139 J. Wade, J. R. Brandt, D. Reger, F. Zinna, K. Y. Amsharov, N. Jux, D. L. Andrews and M. J. Fuchter, *Angew. Chem., Int. Ed.*, 2021, **60**, 222–227.
140 P. Izquierdo-García, J. M. Fernández-García, J. Perles and N. Martín, *J. Am. Chem. Soc.*, 2024, **146**, 34943–34949.
141 S. Li, R. Li, Y.-K. Zhang, S. Wang, B. Ma, B. Zhang and P. An, *Chem. Sci.*, 2023, **14**, 3286–3292.
142 Y. Ju, H. Luo, Z. Li, B. Zheng, J. Xing, X. Chen, L. Huang, G. Nie, B. Zhang, J. Liu and Y. Tan, *Angew. Chem., Int. Ed.*, 2024, **63**, e202402621.

143 D. Yang, K. M. Cheung, Q. Gong, L. Zhang, L. Qiao, X. Chen, Z. Huang and Q. Miao, *Angew. Chem., Int. Ed.*, 2024, **63**, e202402756.
144 G. Venugopal, V. Kumar, A. Badrinarayan Jadhav, S. D. Dongre, A. Khan, R. Gonnade, J. Kumar and S. Santhosh Babu, *Chem. – Eur. J.*, 2024, **30**, e202304169.
145 W. Wang, X. Li, Z. Qi, B. Ji, Z. Wang, S. Wang and J. Xiao, *Org. Lett.*, 2023, **25**, 1343–1347.
146 L. Zhou, H. Liu, J. Tan, C. Liu, X. Cao, A. Narita and Y. Hu, *Chem. – Asian J.*, 2022, **17**, e202200336.
147 L. Wan, J. Wade, X. Shi, S. Xu, M. J. Fuchter and A. J. Campbell, *ACS Appl. Mater. Interfaces*, 2020, **12**, 39471–39478.
148 U. Deori, G. P. Nanda, C. Murawski and P. Rajamalli, *Chem. Sci.*, 2024, **15**, 17739–17759.
149 J. P. Riehl and F. S. Richardson, *Chem. Rev.*, 1986, **86**, 1–16.
150 G. Longhi, E. Castiglioni, J. Koshoubu, G. Mazzeo and S. Abbate, *Chirality*, 2016, **28**, 696–707.
151 R. G. Uceda, C. M. Cruz, S. Míguez-Lago, L. Á. de Cienfuegos, G. Longhi, D. A. Pelta, P. Novoa, A. J. Mota, J. M. Cuerva and D. Miguel, *Angew. Chem., Int. Ed.*, 2024, **63**, e202316696.
152 R. G. Uceda, A. Gijón, S. Míguez-Lago, C. M. Cruz, V. Blanco, F. Fernández-Álvarez, L. Á. de Cienfuegos, M. Molina-Solana, J. Gómez-Romero, D. Miguel, A. J. Mota and J. M. Cuerva, *Angew. Chem., Int. Ed.*, 2024, **63**, e202409998.
153 A. M. Ortuño, P. Reiné, S. Resa, L. Álvarez De Cienfuegos, V. Blanco, J. M. Paredes, A. J. Mota, G. Mazzeo, S. Abbate, J. M. Ugalde, V. Mujica, G. Longhi, D. Miguel and J. M. Cuerva, *Org. Chem. Front.*, 2021, **8**, 5071–5086.
154 T. M. Fukunaga, C. Sawabe, T. Matsuno, J. Takeya, T. Okamoto and H. Isobe, *Angew. Chem., Int. Ed.*, 2021, **60**, 19097–19101.
155 S. Sato, A. Yoshii, S. Takahashi, S. Furumi, M. Takeuchi and H. Isobe, *Proc. Natl. Acad. Sci. U. S. A.*, 2017, **114**, 13097–13101.
156 H. Kubo, T. Hirose, T. Nakashima, T. Kawai, J. Y. Hasegawa and K. Matsuda, *J. Phys. Chem. Lett.*, 2021, **12**, 686–695.
157 D. Meng, T. Zhao, D. Yang, X. Jin and P. Duan, *Mater. Chem. Front.*, 2023, **7**, 3259–3277.
158 J. Wade, J. R. Brandt, D. Reger, F. Zinna, K. Y. Amsharov, N. Jux, D. L. Andrews and M. J. Fuchter, *Angew. Chem., Int. Ed.*, 2021, **60**, 222–227.
159 D. Reger, P. Haines, F. W. Heinemann, D. M. Guldi and N. Jux, *Angew. Chem., Int. Ed.*, 2018, **57**, 5938–5942.
160 J. L. Greenfield, J. Wade, J. R. Brandt, X. Shi, T. J. Penfold and M. J. Fuchter, *Chem. Sci.*, 2021, **12**, 8589–8602.
161 J. M. Moreno-Naranjo, F. Furlan, J. Wang, S. T. J. Ryan, T. Matulaitis, Z. Xu, Q. Zhang, L. Minion, M. Di Girolamo, T. Jávorfi, G. Siligardi, J. Wade, N. Gasparini, E. Zysman-Colman and M. J. Fuchter, *Adv. Mater.*, 2024, **36**, 2402194.
162 Q. Wang, H. Zhu, Y. Tan, J. Hao, T. Ye, H. Tang, Z. Wang, J. Ma, J. Sun, T. Zhang, F. Zheng, W. Zhang, W. Choi, W. C. H. Choy, D. Wu, X. W. Sun, K. Wang, Q. Wang, H. Zhu, Y. Tan, J. Hao, T. Ye, H. Tang, Z. Wang, J. Ma, J. Sun, T. Zhang, F. Zheng, W. Zhang, X. W. Sun, K. Wang, H. W. Choi, W. C. H. Choy and D. Wu, *Adv. Mater.*, 2024, **36**, 2305604.
163 Y. H. Kim, Y. Zhai, H. Lu, X. Pan, C. Xiao, E. A. Gaulding, S. P. Harvey, J. J. Berry, Z. V. Vardeny, J. M. Luther and M. C. Beard, *Science*, 2021, **371**, 1129–1133.
164 M. P. Hautzinger, X. Pan, S. C. Hayden, J. Y. Ye, Q. Jiang, M. J. Wilson, A. J. Phillips, Y. Dong, E. K. Raulerson, I. A. Leahy, C. S. Jiang, J. L. Blackburn, J. M. Luther, Y. Lu, K. Jungjohann, Z. V. Vardeny, J. J. Berry, K. Alberi and M. C. Beard, *Nature*, 2024, **631**, 307–312.
165 L. Zhang, H. X. Wang, S. Li and M. Liu, *Chem. Soc. Rev.*, 2020, **49**, 9095–9120.
166 Y. Gao, C. Ren, X. Lin and T. He, *Front. Chem.*, 2020, **8**, 541567.
167 J. L. Ma, Q. Peng and C. H. Zhao, *Chem. – Eur. J.*, 2019, **25**, 15441–15454.
168 G. Albano, A. Taddeucci, G. Pescitelli and L. Di Bari, *Chem. – Eur. J.*, 2023, **29**, e202301982.
169 D. F. De Rosa, P. Stachelek, D. J. Black and R. Pal, *Nat. Commun.*, 2023, **14**, 1–11.
170 S. P. Morcillo, D. Miguel, L. Álvarez de Cienfuegos, J. Justicia, S. Abbate, E. Castiglioni, C. Bour, M. Ribagorda, D. J. Cárdenas, J. M. Paredes, L. Crovetto, D. Choquesillo-Lazarte, A. J. Mota, M. C. Carreño, G. Longhi and J. M. Cuerva, *Chem. Sci.*, 2016, **7**, 5663–5670.
171 P. Reine, A. G. Campaña, L. Álvarez de Cienfuegos, V. Blanco, S. Abbate, A. J. Mota, G. Longhi, D. Miguel and J. M. Cuerva, *Chem. Commun.*, 2019, **55**, 10685–10688.
172 I. López.Sicilia, A. M. Ortuño, P. Reine, D. Otero, M. R. Martín-Romero, L. Camacho, L. Álvarez de Cienfuegos, A. Orte, J. J. Giner-Casares, D. Miguel and J. M. Cuerva, *J. Mater. Chem. C*, 2023, **11**, 2591–2599.
173 L. Bustillo, T. Laino and T. Rodrigues, *Chem. Sci.*, 2023, **14**, 10378–10384.